García Martínez, A.; Monsalve-Serrano, J.; Lago-Sari, R.; Gaillard, P. (2020). Assessment of a complete truck operating under dual-mode dual-fuel combustion in real life applications: Performance and emissions analysis. Applied Energy. 279:1-21. https://doi.org/10.1016/j.apenergy.2020.115729

Assessment of a complete truck operating under dual-mode dual-fuel combustion in real life applications: performance and emissions analysis

Applied Energy
Volume 279, 1 December 2020, 115729
https://doi.org/10.1016/j.apenergy.2020.115729

Antonio García[a], Javier Monsalve-Serrano[a,*], Rafael Lago Sari[a] and Patrick Gaillard[b]

[a]CMT - Motores Térmicos, Universitat Politècnica de València, Camino de Vera s/n, 46022 Valencia, Spain
[b]Aramco Fuel Research Center, Paris, France

Corresponding author (*):
Dr. Javier Monsalve-Serrano (jamonse1@mot.upv.es)
Phone: +34 963876539
Fax: +34 963876539

Abstract

The dual-mode dual-fuel (DMDF) strategy has been demonstrated to be a potential combustion mode to cover all the engine map with low-to-moderate NOx and soot emissions and high efficiency simultaneously. This can be accomplished by modifying the injection strategy to promote a fully premixed or a dual-fuel diffusive combustion depending on the operating conditions. The main limitation of the DMDF are the high concentrations of unburned hydrocarbons and carbon monoxide coupled with low exhaust temperatures, which can be a challenge for the stock diesel oxidation catalyst (DOC). Moreover, the use of a diffusive combustion combined with high EGR rates to avoid mechanical issues at high load enhances the soot formation, which can compromise the final soot levels in a homologation cycle. To evaluate these aspects, this work studies the performance and emissions of a DMDF truck concept along a WHVC and different in-service conformity cycles through vehicle systems simulations. For both types of cycles, five payloads were tested (0%, 25%, 50%, 75% and 100%) to evaluate the impact of this parameter on the operating points distribution inside the DMDF map. The first results show that the DMDF concept provides engine-out NOx levels below the EUVI regulation at normative payload (50%) with similar fuel consumption than the conventional diesel truck. On the other hand, the engine-out HC and CO emissions exceed their respective limits in all the cases, while the engine-out soot emissions only reach the EUVI levels up to 25% payload. By this reason, the stock DOC and diesel particulate filter from the conventional diesel truck were modelled and fitted to the DMDF truck model. The results evidenced that the use of these two ATS allows to achieve the EUVI limits in terms of tailpipe HC, CO and soot independently on the cycle and payload analyzed. Moreover, considering the tailpipe emissions values achieved with ATS at 50% payload, it can be inferred that both devices could be downsized for the DMDF application as compared to the conventional ATS for diesel applications.

Keywords

Dual-fuel combustion; driving cycle evaluation; in-service conformity tests; aftertreatment system.

1. Introduction

Since the introduction of the European normative for road transportation in 1992, the original equipment manufacturers (OEMs) were forced to develop and update the vehicle technologies to fulfill the challenging scenario aiming to accelerate the shift to sustainable and smart mobility. In 2014, the EUVI normative for medium- and heavy-duty vehicles was introduced in the European union defining reductions of 80% and 60% for NOx and soot emissions, respectively, compared to the previous regulations [1]. Despite of several improvements on the air management system [2], injection systems [3] and piston shape design [4], among others, the engine-out emissions from diesel engines are still far from those of EUVI limits. Therefore, the OEMs relied on the use of complex and costly after treatment systems to be EUVI compliant in their applications. The state-of-the-art aftertreatment systems for distribution vehicles (medium- and heavy-duty) are composed of several devices that addresses the different hazardous pollutants found at the exhaust line of the engine. In this sense, the unburned hydrocarbon and carbon monoxide are dealt by the diesel oxidation catalyst (DOC) [5]. After that, the exhaust gases are filtered in the diesel particulate filter (DPF) removing the solid residues (soot and particulate matter) from the gases [6]. Finally, the selective catalytic reduction (SCR) system decreases the nitrogen oxides (NOx) concentration through the reaction of this specie with the urea fluid (injected by an additional injector) [7]. This complex system works in a coupled way, e.g., the NO_2 production at the DOC during the uHC and CO oxidation is fundamental during the passive regeneration of the DPF as demonstrated in different works [8]. The use of such devices implies drawbacks as the increase in the backpressure [9][10], maintenance and associate working costs as the urea fluid consumption [11].

This scenario encourages the development of techniques that allow the active reduction of the final emissions, i.e., the control of the pollutant formation during the combustion process [12]. In this sense, efforts have been applied to understand [13], model and develop advanced combustion processes[14] to reach this goal. Among the recent advancements, the so-called low temperature combustions (LTC) are one of the major breakthroughs as they allow to achieve low levels of soot and NOx emissions while maintaining or improving the fuel consumption [15]. The LTC concepts address different combustion architectures developed along the years [16][17]. The homogeneous charge compression ignition (HCCI) was a pioneer LTC technique based on the use of a single fuel, with a homogenous and high diluted mixture [18]. This allows to obtain a faster combustion process and low in-cylinder temperatures, reducing the heat transfer losses[19]. Consequently, both emissions, soot and NOx, are inhibited [20], and the efficiency is increased due to the more volumetric combustion process [21]. Nonetheless, this concept presents drawbacks regarding the operating range and combustion control [22]. Reactivity controlled compression ignition (RCCI) combustion demonstrated to be able to overcome the challenges with HCCI by relying on the tailoring of the mixture reactivity [23]. To do this, two fuels with contrasting reactivity

(a low reactivity fuel-LRF and a high reactivity fuel-HRF) are injected by separated injection systems [24]. This allows to extend the operating range while maintaining the benefits [25][26] from the low temperature combustion process [27]. In spite of that, RCCI was still limited to narrow zones inside the engine operating map [28][29], requiring the modification of the combustion mode to allow the operation at full load[30]. Considering this, Benajes et al. proposed a Dual-Mode Dual-Fuel combustion concept (DMDF) [31]. This concept relies on different combustion strategies according to the engine load to cover the complete engine map. From low to medium load, a fully premixed combustion is employed, allowing to explore the benefits of the RCCI concept (low NOx and soot emissions with high efficiency). Once the RCCI combustion start to be limited by the excessive pressure gradients, the injection strategy is modified towards the top dead center (TDC), which enables a dual-fuel diffusive combustion [32]. This is progressively scaled with the engine load, decreasing the premixing levels and increasing the importance of the energy released by the diffusive combustion. Previous steady-state investigations demonstrated that DMDF concept can be engine-out EUVI NOx compliant in most of the operating map. It has been also demonstrated that the DMDF concept can provide similar efficiency than that presented with conventional diesel combustion, even in the case of having 5 points lower of compression ratio[33]. Moreover, it can deal with a wide variety of fuels either as LRF [34][35] or HRF [36] extending its market scaling capabilities. Similar results are found in the literature demonstrating the potential of dual-fuel combustion on using a variety of fuel and the most suitable fuel usage for the concept [37][38][39]. Nonetheless, the air management system limitations require the relaxation of the soot constraints to avoid working in out-of-design conditions at both turbine and compressor. In this sense, from high to full load, the calibration is not able to fulfill neither NOx EUVI limits nor achieve ultra-low soot. Moreover, the use of a PFI strategy enhances the unburned products formation due to the fuel forwarded to the piston crevices during the compression stroke. Dedicated steady-state studies have demonstrated that this can be a challenge for the conventional aftertreatment system [40] (mainly at fully premixed combustion) because the DMDF engine-out products are orders of magnitude higher than those from CDC and the lower exhaust temperature from the LTC combustion [41]. Investigation with dual-fuel concepts consisting on ignition support from an electrical discharge demonstrated that the spark energy may provide benefits at low engine load, reducing the cyclic variability and the concentration of unburned products in lean conditions similar to those verified in the DMDF concept[42][43][44].

Steady-state results are useful to evaluate the technology potential and to understand the dependencies between the governing parameters of the problem in discussion. Nonetheless, the technology development requires evaluations at representative working conditions that differ according to the device applications. Medium- and heavy-duty transportation must fulfill specific emissions targets under different driving cycles that address representative operating conditions and time usage of the engine map of those verified in real applications. Therefore, it should be expected that the engine map zones will have a different weight on the global results. Considering the characteristics of the DMDF combustion maps, it is clear that this evaluation approach should be employed to guarantee a proper assessment of the contrasting behaviors obtained according to the combustion strategy used. This will allow to position the proposed combustion mode in the current EUVI normative. It should be remarked that the truck

homologation procedure also requires the evaluation of in-service conditions with specific emission limits. The literature review allows to verify that the investigation in real scenarios is usually less common than the steady-state assessment due to the significant amount of required data for both validation and evaluation steps. In the case of the DMDF concept valuation, there is no report of similar investigations in the literature up to the date.

Considering the previous results for HC and CO, it is evident that both emissions will require a dedicated aftertreatment system to be EUVI compliant. Moreover, the use of a low pressure EGR system would require the pre-filtration of the exhaust gases prior entering into the inlet line to avoid the compressor blades damage[45]. It should be also remarked that the soot levels produced at high engine load could be high enough to compromise the combustion concept in terms of EUVI soot levels. Therefore, the stock engine DOC and DPF should be also evaluated to extend the analysis from engine-out up to tailpipe emissions, providing and overview on the aftertreatment performance on transient applications. In this sense, this investigation proposes the transient evaluation through driving cycles of the DMDF concept on a medium-duty commercial engine platform in terms of performance and both engine out and tailpipe emissions, stressing its capabilities and challenges on normative and real driving conditions. To do this, a complete longitudinal truck model equipped with the engine platform used to develop the combustion concept was modelled and validated in GT-drive in terms of fuel consumption and emissions to guarantee a proper comparison with respect to the normative values. Moreover, the original aftertreatment system for unburned hydrocarbons and carbon monoxide as well as soot emissions were modelled and validated to investigate the impact of the DMDF combustion on their performance and to evaluate the potential of DMDF to provide EUVI compliant aftertreatment emissions at tailpipe levels. The World harmonized vehicle cycle (WHVC) was used as reference driving cycle to perform the evaluation under normative conditions. Nonetheless, giving the importance of the in-service conformity (ISC) tests on a truck homologation procedure, an additional ISC cycle was included in the analysis. Finally, two real drive conditions were added to the cycle data base, one of them is dedicated to evaluate the DMDF concept for urban truck applications and the other allows a specific fuel consumption evaluation for comparison purposes. For each cycle, five payloads were tested (0%, 25%, 50%, 75% and 100%) to evaluate the impact of this parameter on the operating points distribution inside the DMDF map and therefore on the global results. The results obtained may be used as benchmark for dual-fuel engines for medium-duty transportation as also stress the main benefits and drawbacks that should be considered in this specific research line.

2. Materials and methods

This section describes the experimental facilities, testing methodologies and the numerical models used during the investigation.

2.1. Engine and test cell description

The engine used in this investigation consists of a medium-duty, four stroke, multi-cylinder platform. Extensive works were previously developed in its single-cylinder version to understand and achieve the current combustion concept herein presented [46]. From these previous investigations, it was suggested that the geometric

compression ratio should be reduced from 17.5 to 12.75:1 to realize full load operation with dual-fuel combustion. This modification allowed to reduce the mechanical demand verified at high load conditions from the premixed combustion (pressure gradients). Moreover, a low pressure (LP) exhaust gas recirculation (EGR) system was installed to extend the EGR amounts that can be done while maintaining a proper energy flow through the turbine to allow achieving the desired boost pressure. Table 1 presents the main characteristics of the engine used during the investigation.

Table 1. Main engine characteristics.

Engine Type	4 stroke, 4 valves, direct injection
Number of cylinders [-]	6
Displaced volume [cm^3]	7700
Stroke [mm]	135
Bore [mm]	110
Piston bowl geometry [-]	Bathtub
Compression ratio [-]	12.75:1
Rated power [kW]	235 @ 2100 rpm
Rated torque [Nm]	1200 @ 1050-1600 rpm

Figure 1 depicts a scheme of the bench test in which the engine was installed. It comprehends control, monitoring and acquisition systems to allow a proper assessment of each operating condition. The engine was fully instrumented with average and instantaneous sensors. The last were used to monitor and acquire the intake, in-cylinder and exhaust pressures while the average sensors allowed to record temperature and pressure values at different locations. These signals were acquired by means of a NI PXIe 1071 board, which also enabled the online assessment of the combustion process by means of a heat release analysis. In this sense, the main combustion metrics as CA10, CA50 and CA90 as well as the heat release profile could be observed during the engine calibration. These combustion metrics were obtained from integrating the instantaneous heat release rate and referencing the crank angle at which the mass fraction burned was 10, 50 and 90, respectively. In addition, fuel and air mass flows were measured by means of two AVL733S balances (one for each fuel) and an Elster RVG G100 sensor, respectively.

The engine control was split between two systems: the original engine control unit (ECU) and a dedicated control developed in LabVIEW. The original ECU was used to control the injection pressure, turbocharger rack position and high pressure EGR by means of an ATI Vision software by Accurate Technologies Inc. However, the injector actuation (for both HRF and LRF) was switched to the LabVIEW routine. This routine was also able to control the additional low pressure EGR system. The engine speed and load were controlled by means of an AVL active dynamometer using the AVL Puma interface which is an integrated solution for the engine load control and data acquisition.

The combustion products from each operating condition were measured by dedicated measurement devices. A five-gas Horiba MEXA-7100 DEGR analyzer was used to quantify the unburned hydrocarbon concentration by means of flame ionization detection, O_2 by paramagnetic principle, CO from non-dispersive infrared and both NO

and NO_2 by chemiluminescence. Smoke emissions were measured by an AVL 415S smoke meter in filter smoke number (FSN) units. Before that, the FSN measurements were correlated to mass considering the methodology proposed by [47]. It should be remarked that the soot mass herein presented does not comprehend the total particulate mass, once the AVL 415 S measurement principle is not able to account for the condensable hydrocarbons, which represents a significant portion of the particulate mass in DMDF combustion. Due to this reason, even in the case of having soot emissions lower than 0.01 g/kWh, it cannot be assured that EUVI is achieved for particulate matter. Table 3 summarizes the accuracy of the main elements of the test cell.

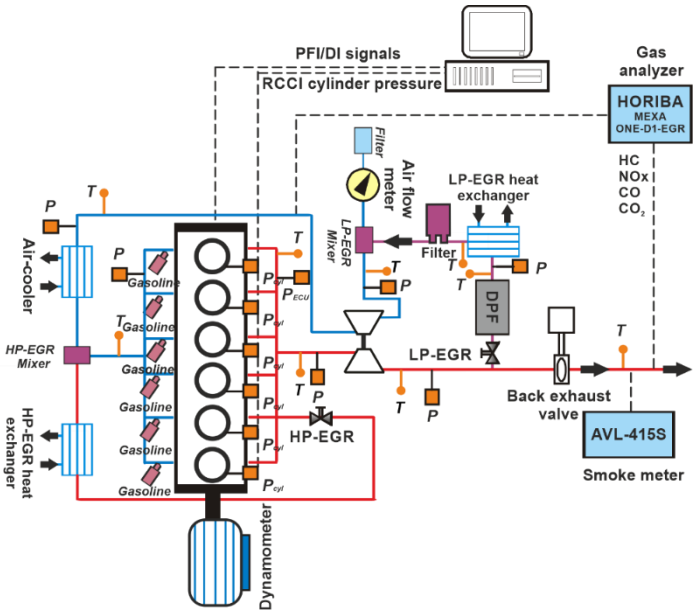

Figure 1. Configuration of the test cell used during the experiments.

Table 3. Accuracy of the instrumentation used in this work.

Variable measured	Device	Manufacturer / model	Accuracy
In-cylinder pressure	Piezoelectric transducer	Kistler / 6125C	±1.2 %
Intake/exhaust pressure	Piezoresistive transducers	Kistler / 4045A	±25 mbar
Temperature in settling chambers and manifolds	Thermocouple	TC direct / type K	±2.5 °C
Crank angle, engine speed	Encoder	AVL / 364	±0.02 CAD
NOx, CO, HC, O_2, CO_2	Gas analyzer	HORIBA / MEXA 7100 DEGR	4%
FSN	Smoke meter	AVL / 415	±0.025 FSN
Gasoline/diesel fuel mass flow	Fuel balances	AVL / 733S	±0.2%
Air mass flow	Air flow meter	Elster / RVG G100	±0.1%

2.2. Fuels and injection systems characteristics

Recent investigations demonstrated that the use of advanced fuels can be an alternative to reduce the CO_2 impact of the DMDF combustion concept. Nonetheless, most of them cannot be considered drop-in fuels, requiring significant modifications on the engine platform to allow their use. Moreover, the unstable distribution network, low availability

and market volatility are challenges that must be solved prior to a scalable use. In this sense, this work focus on the use of gasoline and diesel as low reactivity and high reactivity fuels, respectively, aiming to extend their current application on internal combustion engines with advanced combustion modes. The main characteristics of the fuels used in this investigation are presented in table 4.

Table 4. Physical and chemical properties of the fuels used in the investigation.

	EN 590 diesel	EN 228 gasoline
Density [kg/m^3] (T= 15 °C)	842	720
Viscosity [mm^2/s] (T= 40 °C)	2.929	0.545
RON [-]	-	95.6
MON [-]	-	85.7
Cetane number [-]	51	-
Lower heating value [MJ/kg]	42.50	42.4

To do this, a dedicated injection system was designed to inject the low reactivity fuel consisting of six high-flow port fuel injectors (PFI) installed in the original intake manifold. In addition, a low-pressure pump was used, maintaining the injection pressure at 6 bar during the investigation. The stock common-rail fuel injection system was maintained to inject the HRF (diesel), consisting of 6 centrally located solenoid injectors. The characteristics of both PFI and DI systems are presented in Table 5.

Table 5. Characteristics of the direct and port fuel injectors.

Direct injector		Port fuel injector	
Actuation Type [-]	Solenoid	Injector Style [-]	Saturated
Steady flow rate @ 100 bar [cm^3/min]	1300	Steady flow rate @ 3 bar [cm^3/min]	980
Included spray angle [°]	150	Included Spray Angle [°]	30
Number of holes [-]	7	Injection Strategy [-]	single
Hole diameter [µm]	177	Start of Injection [CAD ATDC]	340
Maximum injection pressure [bar]	2500	Maximum injection pressure [bar]	5.5

2.3. Calibration methodology and experimental maps.

The engine testing was performed following a specific calibration procedure, aiming to optimize each operating condition in terms of brake specific fuel consumption while maintaining the emission under stablished constraints. More details about the calibration methodology can be found at [48]. Figure 2 summarizes the emissions constraints that were obeyed during the calibration and the respective injection strategy. At first, EUVI engine-out NOx with soot lower than 0.01 g/kWh were aimed. This was accomplished promoting a fully premixed combustion, mitigating the fuel rich and the high temperature zones at the same time [49]. Nonetheless, this strategy could not be extended to loads higher than 60% due to the significant increase of the pressure gradients. In this sense, the injection strategy was modified, delayed the HRF injection to enable a flatter HRR profile, i.e., to distribute the energy in a large period, maintaining the pressure gradients at feasible levels. Consequently, the mixing time is reduced, enhancing the soot formation. For these conditions, only NOx emissions were maintained under the pre-established targets. As the engine load was increased, the

turbocharger approached to its limiting boundary conditions specified by the OEM. The turbine inlet temperature and pressure as well as the compressor outlet temperature were out of design limits, preventing the fulfillment of EUVI NOx emissions. Therefore, the constraints were relaxed to achieve full load operation and provide similar power output than the original platform. The characteristic heat release profiles of each one of the combustion strategies are presented in Figure 2(b). As it can be seen, the fully premixed profile is characterized by a fast and uniform combustion process which is known by providing high fuel-to-work conversion efficiencies. As the injection strategy is modified, a second heat release peak can be noticed, indicating the existence of a diffusive combustion process. As the engine load is increased, more significant is the second combustion phase, allowing to conclude that its objective is to provide the remaining energy to achieve the desired engine load.

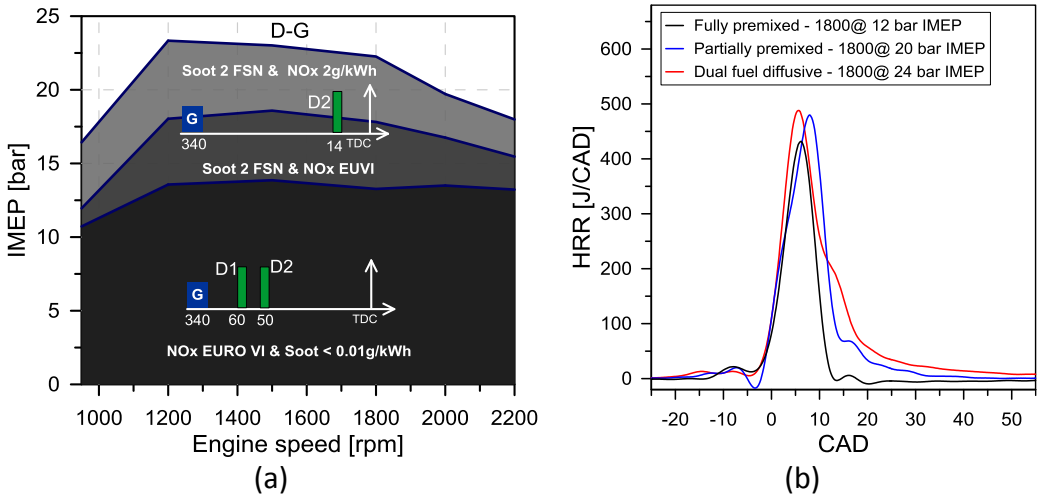

Figure 2. (a) schematic representation of the injection strategy along the calibration map (b) characteristic heat release rates for points in the different zones of Figure 2(a).

Figure 3 depicts the efficiency map obtained with the previous strategy. More details and a deeper description of the results can be found in a previous works from the authors[33]. It can be noted that brake efficiency values higher than 40% could be obtained for most of the calibration map. Moreover, the maximum efficiency point locates on the fully premixed combustion zone, where the heat transfer losses are minimized.

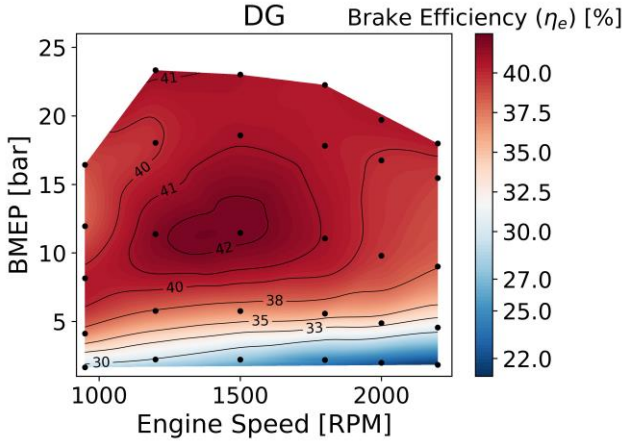

Figure 3. Brake efficiency map obtained with the Dual-Mode Dual-Fuel combustion concept.

The NOx and soot emission maps reflect the limits imposed during the calibration strategy, as it can be visualized in Figure 4. Regarding the NOx emissions, most of the calibration map is EUVI compliant, i.e., lower than the normative limit of 0.4 g/kWh for steady-state conditions. This could be achieved combining high degree of premixed combustion coupled with massive EGR amounts. While the premixed combustion was employed, both soot and NOx emissions were suppressed. Nonetheless, as the load was increased the NOx emissions were maintained under EUVI limits at the cost of exceeding the soot constraints by the lack of oxygen from the high EGR levels. At near full load conditions, both emissions are relaxed to provide similar power output than the stock CDC engine.

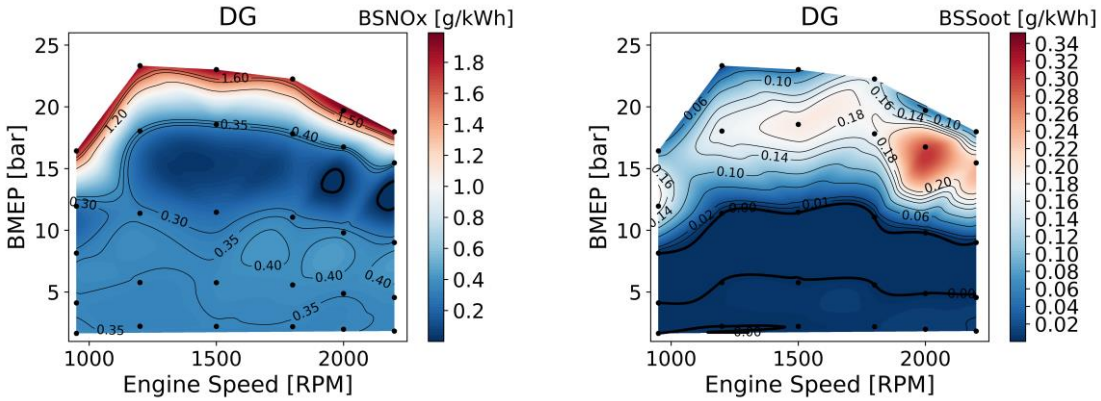

Figure 4. (a) Brake specific nitrogen oxides and (b) brake specific soot maps obtained with the Dual-Mode Dual-Fuel combustion concept.

As it can be seen in Figure 5, both HC and CO emissions present penalizations over the whole calibration map due to the low combustion efficiency. The early fuel injections are generally forwarded to the piston gaps during the compression stroke. These regions are characterized by low characteristic diameters where the oxidation cannot be sustained [50]. Therefore, most of the fuel that enters these zones is not burned during the combustion process. The HC maps corroborates with this assumption. As it can be seen, the HC emissions seems to be scaled with the premixing degree, being higher at fully premixed conditions and steeply decreasing as the diffusive part is more prominent.

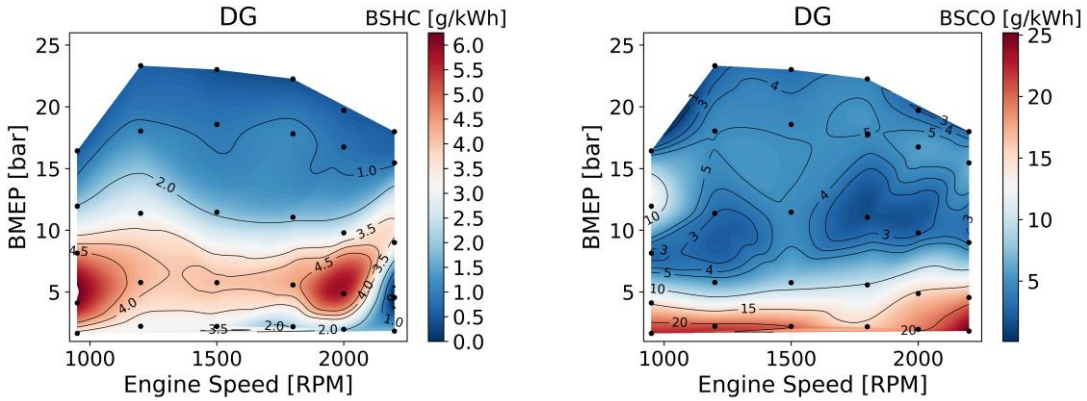

Figure 5. (a) Brake specific unburned hydrocarbons and (b) brake specific carbon monoxide maps obtained with the Dual-Mode Dual-Fuel combustion concept.

2.4. Truck numerical model

As previously stressed in the introduction section, transient evaluations are required by the normative during the truck homologation process. During the transient operation, the engine can achieve different operating conditions, creating a cloud of points which will define the importance of each zone, providing cumulative and averaged results at the end of the cycle. To emulate these effects, a complete vehicle numerical model was developed in GT-Drive considering a commercial truck equipped with the engine previously described. Figure 6 depicts the GT-Drive model developed. It consists of an engine object, transmission and vehicle. This last comprehends the cabin dimensions, drag coefficients, axle geometry, differential setup, number of axles, etc. All these characteristics are set according to the OEM references. The truck as well as transmission characteristics can be found at [51]. The vehicle emulation is based on conventional longitudinal vehicle dynamics. This approach considers the different sources of power requirements that could appear during a real application as drag, inertial and friction powers.

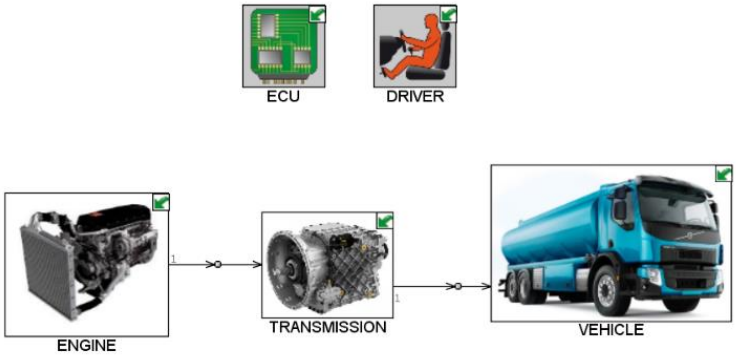

Figure 6. GT-Drive model for the VOLVO FE 350 truck.

Equation 1 presents the governing equation that should be solved for each simulation timestep where I_{trans1} and I_{trans2} present the inertia in the input and output of transmission system. Likewise, I_{dsh} and I_{axl} are driveshaft and axle moment of inertia. R_d and R_t are terms of final drive and transmission ratio for each gear. Vehicle speed (ω_{drv}) at the instant of time (t) is directly related to the wheel radius (r_{whl}) and vehicle mass (M_{veh}). Aerodynamic forces (F_d), rolling resistance forces (F_{rol}) and gravity forces (F_{grd}) are considered in the last term of Equation 1. Detailed information can be found at [52].

$$\begin{aligned}\tau_{vehicle} = &\left[I_{trans1} + \frac{I_{trans2}}{R_t^2} + \frac{I_{dsh}}{R_t^2} + \frac{I_{axl}}{(R_d^2)(R_t^2)} + \frac{(M_{veh})(r_{whl}^2)}{(R_d^2)(R_t^2)}\right]\frac{d\omega_{drv}}{dt} \\ &- \left[\frac{I_{trans2}}{R_t^3} + \frac{I_{dsh}}{R_t^3} + \frac{I_{axl}}{(R_d^2)(R_t^3)} + \frac{(M_{veh})(r_{whl}^2)}{(R_d^2)(R_t^3)}\right]\omega_{drv}\frac{dR_t}{dt} \\ &+ \left[\frac{F_{aer} + F_{rol} + F_{grd}}{R_d R_t}\right] r_{whl}\end{aligned} \quad (1)$$

The maps described in section 2.3 are used as boundary conditions at the engine object. During the driving calculation, Equation 1 will provide a representative BMEP requirement, while the vehicle velocity will dictate the engine speed considering the different transmission ratios. For each time step, a BMEP and engine speed pair will be

given to the engine object which will provide an interpolated value of the performance and emissions produced for this specific condition. It should be argued that the thermodynamic transient that exist in real application cannot be capture in this approach. Therefore, an error quantification was made to account the reliability of the developed model for both working devices (transmission setup, clutch, axles) as well as performance and emissions. To do this, specific tests with the modelled truck were performed, measuring fuel consumption, rotational speed, and torque at different truck sites. The same driving conditions were replicated in GT-Drive and compared to the experimental results. It should be noted that these results are achieved with a commercial truck equipped with a conventional diesel engine.

Figure 7 depicts the resultant engine speed and engine torque that are demanded during the driving cycle compared with the experimental results. As described, the engine torque is a consequence of the different forces that acts over the truck while the engine speed is defined by the driving cycle velocity profile and the different transmission along the truck up to the engine. From Figure 7, it can be concluded that both parameters are well captured by the model, presenting similar qualitative and quantitative results than the experimental data during the driving cycle. This allows to affirm that the engine model is running on the same operating condition than those from the experiments.

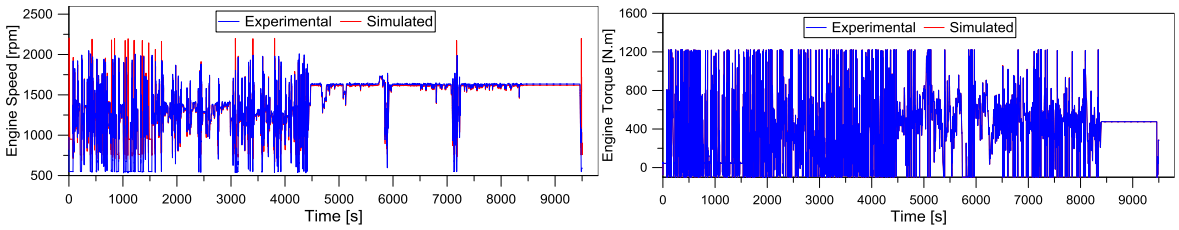

Figure 7. Experimental and simulated engine speed (a) and engine torque (b) for the driving cycle evaluated operating in conventional diesel combustion.

The same parameters (speed and torque) were also evaluated at the axle output, prior to be scaled by the axle gear ratio and the transmission system. This guarantees that speed and torque are properly modelled at the both ends of the system: engine and axle output. Figure 8 depicts the axle speed and torque results. It can be suggested that both are well represented by the computational model. Slightly differences are verified at the axle torque in form of spikes, which can be resulted from different parts (e.g. clutch slip).

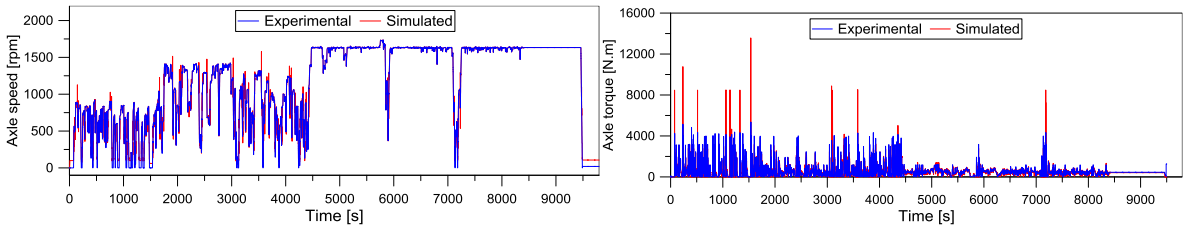

Figure 8. Experimental and simulated axle speed (a) and axle torque (b) for the driving cycle evaluated operating in conventional diesel combustion.

Finally, the numerical and experimental instantaneous fuel consumption results are compared in Figure 9. As it can be seen, the steady-state interpolation seems to be able to capture the transient experimental trends as well as the absolute values.

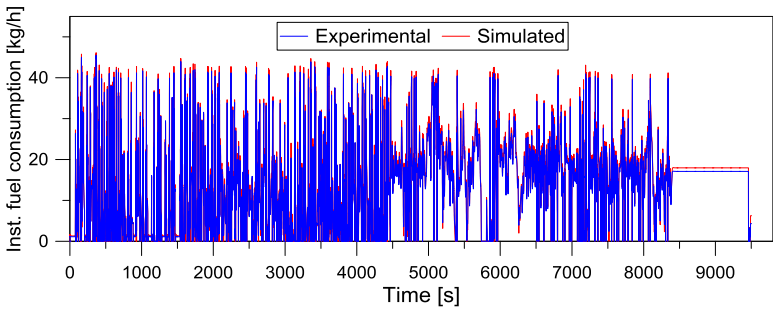

Figure 9. Experimental and simulated instantaneous fuel consumption for the driving cycle evaluated operating in conventional diesel combustion.

Despite of the general accuracy demonstrated in Figure 9, some slightly deviations can be noted as the ones in the end of the cycle. This can be not only consequence of the approach that has been used as also differences from the engine, lifetime, etc. In any case, the cumulative fuel consumption calculated considering both results (numerical and experimental) is presented in Figure 10. As it can be seen, the two cumulative profiles are attached during the urban phase of the cycle. As the truck velocity is increased and so the engine load, the differences start to appear. Nonetheless, the maximum difference achieved is lower than 5%. It should be kept in mind that the experimental results (truck measurements and steady-state maps) come from a different engine units, where measurement techniques with different uncertainties are used. In this sense, the differences verified at the end of the cycle cannot be only attributed to the numerical model.

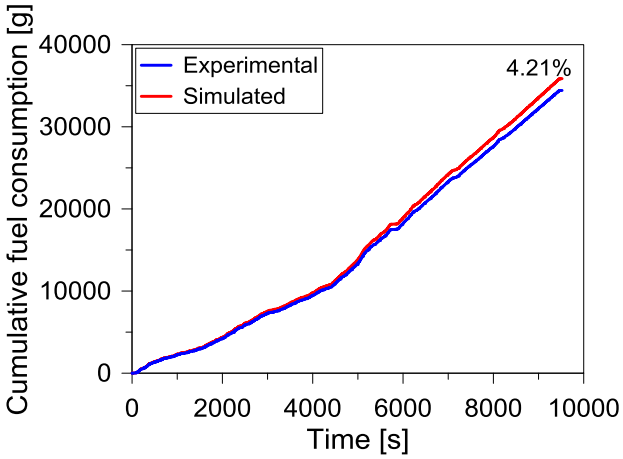

Figure 10. Experimental and simulated cumulative fuel consumption along the driving cycle.

To validate the model in terms of emissions, transient cycles were performed in a test cell with the DMDF engine, and then compared with the results from the simulations. This approach is reasonable since the truck characteristics are already validated. To do this, it was proposed a similar transient step than those presented in the supplementary engine tests (SET), considering the recommendations for the transition time, engine speed limits, etc. Figure 11 presents the step used for the emissions evaluation. As the steady state maps were measured in warm conditions, a pre-engine heating step was placed in the first 200 s. In this sense, the measurements were started after this first interval, avoiding the divergences in the raw emissions caused by the temperature dynamics.

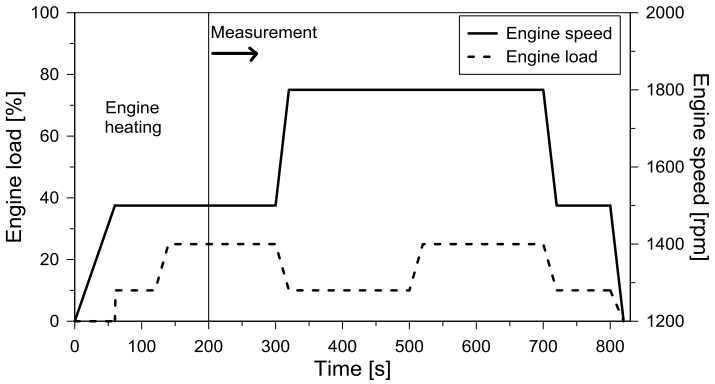

Figure 11. Transient cycle to compare and quantify the experimental and numerical emissions.

The step results are depicted in Figure 12. It should be stated that transient soot emissions are not reported since it requires specific measurement devices. Figure 12 (a) illustrates the NOx cumulative results along the step time. As it can be seen, low variations (lower than 2%) are experienced even in the case of having low absolute concentration. Literature results suggested that NOx emissions can be properly described by this tabulated approach once the engine is operating at warm conditions [53]. Both HC and CO emissions present higher variations than those observed in NOx emissions. These emissions are not only related with the maximum temperature achieved in the burned zone, but also with the wall temperatures, where the reaction quenching is enhanced. This can be appreciated in the cumulative profiles. The differences tend to be minimized if a larger time interval is considered to start the measurements, where the engine thermal conditions are closer to a steady-state point.

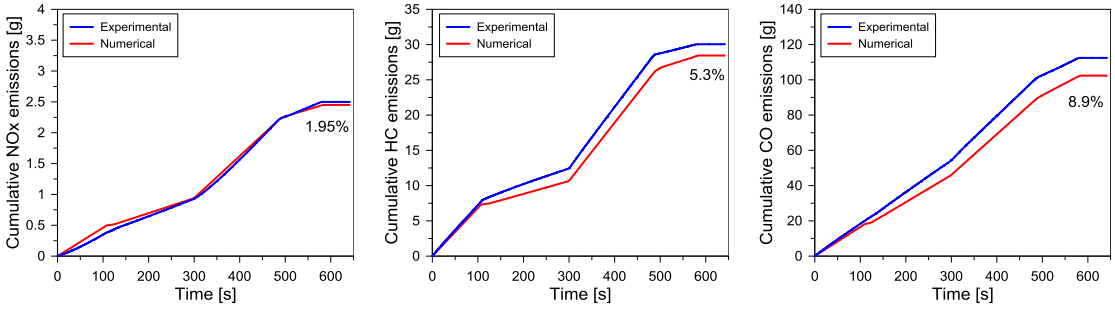

Figure 12. Experimental and simulated cumulative (a) nitrogen oxides, (b) unburned hydrocarbon and (c) carbon monoxide emissions.

2.5. Driving cycles

The different driving cycles used for the investigation of the combustion concept are presented from Figure 13 to Figure 16. As it can be seen, they present several velocities profiles that represent some of the different applications in which the medium trucks are used. Figure 13 presents the world harmonized vehicle cycle which considers three different phases: urban, rural and highway, being used as normative driving cycle.

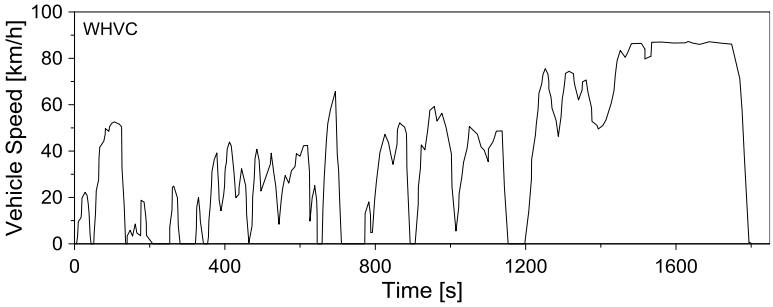

Figure 13. Velocity profile of the world harmonized vehicle cycle.

The last three driving cycles comprises in-service conformity, real driving and fuel consumption evaluation conditions that are generally used to homologation purposes [54] and to performance comparison. Figure 14 presents a full ISC cycle under the normative requirements, which provides a similar profile than that presented in the WHVC cycle. Nonetheless, its duration is more than 4.5 times than the WHVC and presents zero velocity points even in the highway phase, which provides different acceleration profiles than those form the WHVC.

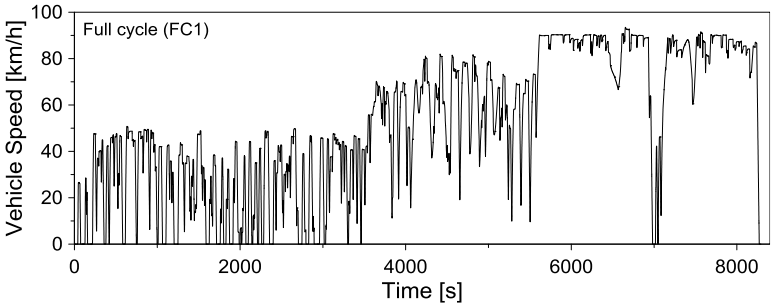

Figure 14. Velocity profile of the in-service conformity driving cycle.

Figure 15 addresses an urban real driving cycle, which represents the utilization of commercial trucks to perform daily tasks in the city as product delivery, garbage collection, etc. As it can be seen, it is composed by a high frequency of accelerations and it has a maximum value around 70 km/h.

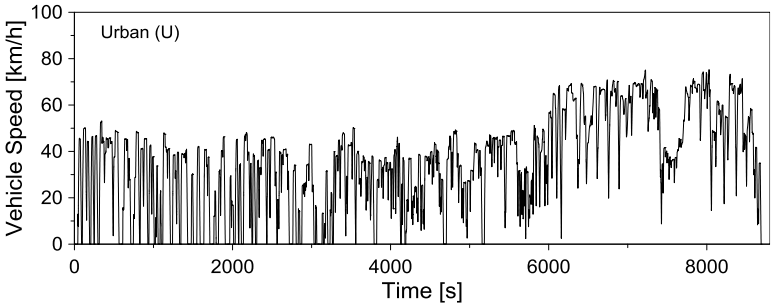

Figure 15. Velocity profile of urban real driving cycle.

Finally, a simplified driving cycle for fuel consumption evaluation purposes is presented. As it is evidenced, there a reduced number of accelerations, with a duration slightly higher than the WHVC.

A specific nomenclature for the driving cycles was developed to simplify the data presentation: ISC_FC for the full cycle case, Urban for the urban real driving case and FCEC for the last driving cycle, respectively.

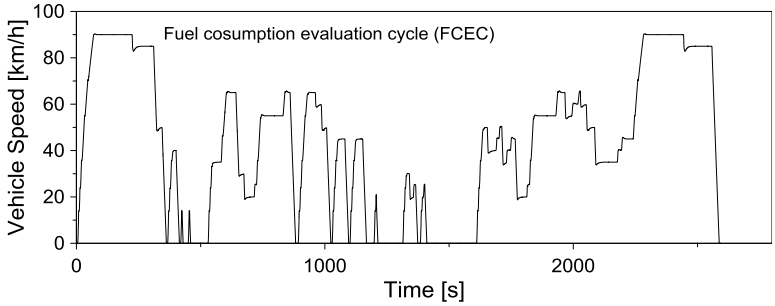

Figure 16. Velocity profile of the fuel consumption evaluation cycle.

2.6. Diesel oxidation catalyst modelling and validation

Several authors dedicated their work on developing efficient and accurate models to describe the oxidation of unburned products in oxidation catalysts according to the different dominant parameters. Among the significant contributions in this field, Sampara and Bisset were able to develop a simplified reaction mechanism which demonstrated good accuracy and fast solution time [55][56]. The global Kinect mechanism is composed of the reactions presented in Table 6:

Table 6. Sampara and Bisset global kinetics mechanism for DOC operation.

$CO + 0.5O_2 = CO_2$	reaction 1
$C_3H_6 + 4.5O_2 = CO_2 + H_2O$	reaction 2
$C_3H_8 + 0.5O_2 = CO_2 + H_2O$	reaction 3
$DF_1 + 19.4O_2 = 13.5CO_2 + 11.8H_2O$	reaction 4
$H_2 + 0.5O_2 = H_2O$	reaction 5
$NO + 0.5O_2 = NO_2$	reaction 6
$Z + DF_1 = ZDF_1$	reaction 7
$ZDF_1 = Z + DF_1$	reaction 8

Each equation has a pre-exponential factor and an activation energy that should be calibrated according to the combustion type, species range, characteristics velocity, etc. In this sense, a calibration step was carried prior to the driving cycle simulation. First, a dataset was chosen from the experimental database considering the operating conditions that represent a monotonically increase of temperature, to determine characteristics as the light-off point. The operating condition used for the calibration procedure are presented in Table 7

Table 7. Dataset used to the DOC calibration.

Op. Cond.	ES [rpm]	PME [bar]	m [g/s]	T_DOC$_{inlet}$ [°C]	HC [ppm]	CO [ppm]	O_2 [%]	HC$_{conv}$ [%]	CO$_{conv}$ [%]
1	1200	2.15	43.46	176	432	2436	12.08	42.80	12.04
2	1800	2.10	75.72	208	742	1433	12.88	89.90	99.69
3	2000	1.91	81.00	214	720	1501	12.31	91.61	99.72
4	2200	1.78	85.25	227	329	2335	10.88	92.20	99.79
5	1200	5.66	57.48	256	3912	1420	8.62	96.47	99.88
6	1500	5.74	76.90	273	3432	1737	8.95	96.78	99.64

A detailed model of the DOC was developed considering the measurement locations of species, temperature and pressure as boundaries for the model. This allows to isolate the device and to simplify the calculation routine, since complex phenomena as the combustion process are not modelled. Figure 17 presents the DOC model developed in GT Power. The inlet part allows to set the species concentrations before the DOC as well as the total mass and temperature values. The catalyst part addresses the geometric characteristics as the wash coat width, length and channels density, among others, while the DOC englobes the chemical reactions from the Kinect mechanism. The exhaust composition was approximated by an 11 species reactions considering the routine proposed by [57]

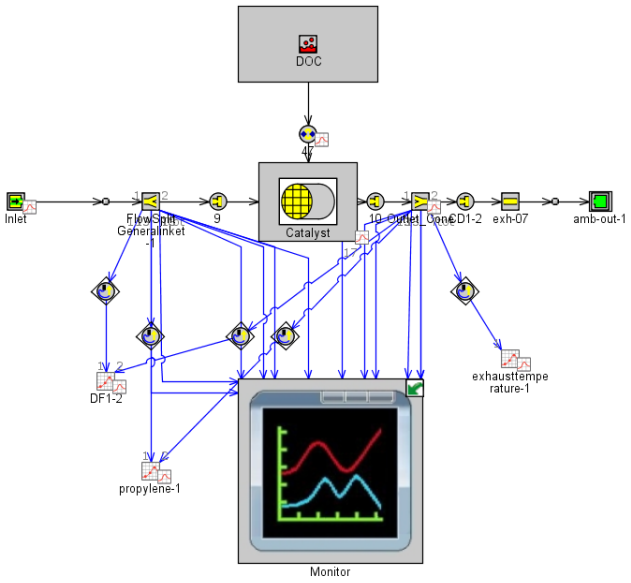

Figure 17. Diesel oxidation catalyst model developed in GT-Power.

Once the model was set, an optimization tool from Gamma technologies based on genetic algorithm and logarithm space searching was used to determine the global optimum for the reaction constants of the previous equations. Detailed information about the methodology used in this step can be found in [58]. Figure 18 presents the results obtained considering the best set of pre-exponential factors and energy of

activation for each one of the global reactions. As it can be seen, the numerical results for both HC and CO follow closely those from the experiments. The most noticeable differences are perceived at low temperatures, lower than the light-off conditions. Literature results demonstrates that these are the most challenging conditions to be modeled for internal combustion engines, since these low engine-out temperatures are generally found in low load points, where the combustion variability is high, promoting significant differences in the flow and composition of the exhaust gases [59]. In general, the behavior of the conversion efficiency is well captured by the numerical model, with low deviations even in the case of having low temperatures and conversion efficiencies.

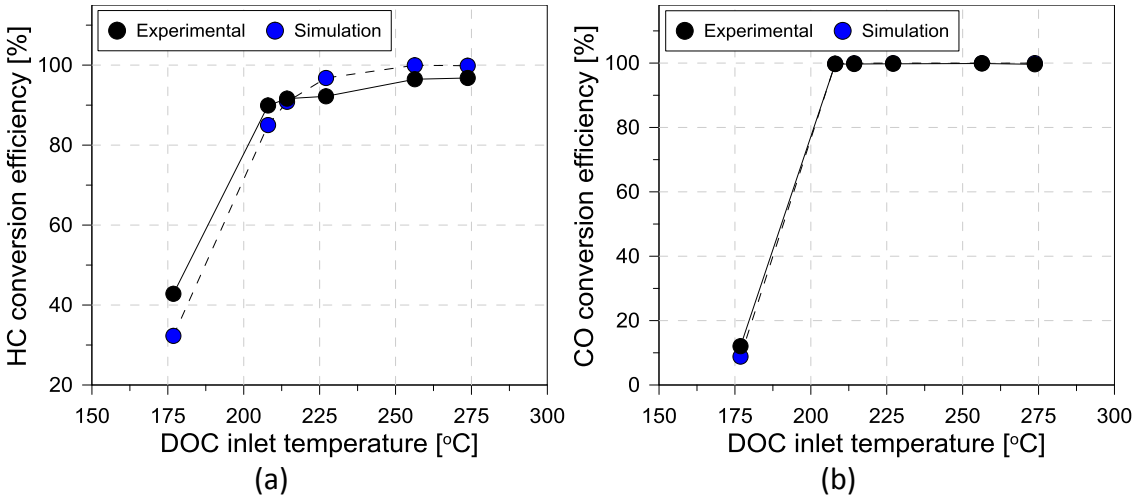

Figure 18. Experimental *vs* simulated conversion efficiencies for (a) unburned hydrocarbon and (b) carbon monoxide considering the best set of calibration constants for the calibration points.

After calibrating the model, an extra dataset was used to validate the set of constants found by the optimizer. Therefore, 13 operating conditions addressing conditions with low and high conversion efficiency for both HC and CO were used. As the Figure 19 shows, the model can properly predict the conversion efficiency at steady-state conditions, presenting acceptable deviations from the experimental results.

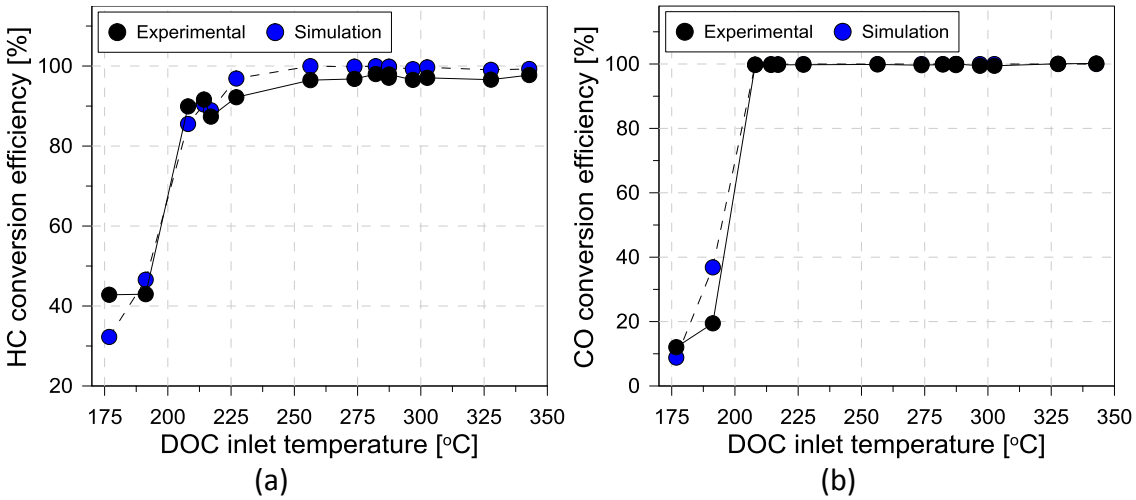

Figure 19. Experimental *vs* simulated conversion efficiencies for (a) unburned hydrocarbon and (b) carbon monoxide considering the best set of calibration constants for the validation dataset.

Despite of the good results at steady-state conditions, the main goal of the investigation is to assess the engine-out and tailpipe emissions at transient conditions. Therefore, the DOC model should be assessed in similar conditions. To do this, the boundary conditions

from an experimental step from previous works was used and the numerical results were confronted with those from the experiments [41]. Figure 20 presents the results for both HC and CO emissions. As it can be seen, the numerical model is able to predict the conversion efficiency of both pollutants in most of the transient step. A significant variation verified at 400 s, where the engine speed is modified in the experiments. This can be attributed to the slow response of the thermocouple to the temperature transients, which could result in deviations on the boundary conditions. The DOC inlet temperature values are shown in Figure 21, where the thermal behavior of the DOC was compared to those from the experiments. The proper prediction of this temperature should be guaranteed since it is used as boundary condition for the DPF assessment in the same way as the species concentrations.

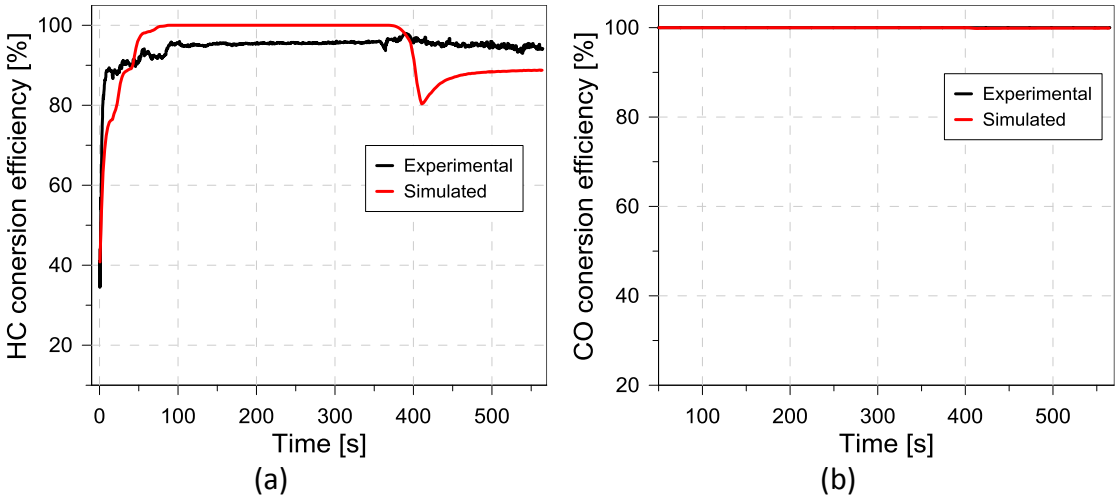

Figure 20. Comparison between experimental and simulated conversion efficiency for (a) unburned hydrocarbon and (b) carbon monoxide for transient conditions.

As it can be seen in Figure 21, the calculated temperature can deliver similar results to those from the experiments. The maximum deviations are evidenced at the engine speed transitions (8-10%). After that, the values tend to be closer, experiencing differences lower than 5%. This supports the assumption that a fast thermocouple should be used to avoid the influence of the thermal inertia and slow dynamics of the thermocouples on the boundary conditions for the transient simulations. In spite of these issues, the temperature differences are maintained in acceptable levels allowing to conclude that the DOC model is able to predict the conversion efficiency of the species as well as the thermal phenomena that take place inside the device.

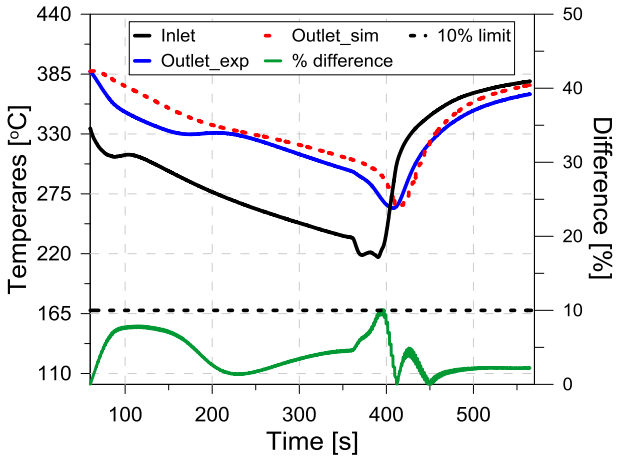

Figure 21. Inlet temperature and comparison between experimental and simulated temperature results at the DOC outlet.

2.7. DPF modelling approach

Previous results suggested that the DMDF combustion concept based on diesel and gasoline as HRF and LRF, respectively, is prone to produce soot at specific operating conditions where the air management system starts to be limited [48]. Moreover, the use of low pressure EGR system would require a filtration of the exhaust gas particles prior to entering the compressor to avoid damaging the compressor blades. In this sense, it can be stated that the DPF system would remain as an important device in this application. Based on this, it was included in the aftertreatment system model to evaluate its performance with respect to the different engine loads and driving cycles. To do this, an in-house DPF model developed by Piqueras et al. [60] was included in the GT-drive simulations, considering the DOC outlet conditions as boundaries to the DPF assessment.. Briefly, the PF models solves the governing equations of momentum, mass and energy. They are simplified assuming a non-homoentropic one-dimensional unsteady compressible flow in inlet and outlet channels. Each one of the equations is solved by means of finite difference, closed by the gas state equation. Darcy's law is considered to calculate the pressure drop between the inlet and the outlet channels. The regeneration models are included, interacting with the conservation equations in several ways as the composition of the gases and the mass balance of soot. Moreover, the regeneration process is considered a quasi-steady process with negligible impact of the diffusive transport across the porous media. The detailed formulation, solution scheme and specificities of the DPF model can be found in [61].

The analysis presented in [41] was used as dataset to calibrate the different phenomena that takes place inside the PF, as the soot loading, passive and active regeneration for the DMDF concept. A reduced number of calibration constants are adjusted compared to the previous described DOC model and are mainly related to the oxygen path regeneration and the flow effects description. In this sense, the use of time expensive calibration methods as genetic algorithms is not justified, allowing to rely on manual adjustment without losing accuracy on the solution. This can be inferred from the analysis of the next comparison between the experimental and predicted results. Figure 22 (a) presents the results obtained considering a DPF loading for 15 hours. As it can be seen, the model is able to reproduce the complex phenomena along the time, providing similar accumulated soot values than those from the experiments. This conclusion can also be extended to Figure 22 (b), where the active regeneration results are presented. This means that the model is able to reproduce the soot accumulation process as well as the combined regeneration by NO_2 and oxygen. Therefore, the calibrated model was coupled to the global GT-drive model enabling a complete analysis of the DMDF performance as well as the emissions before and after the DPF.

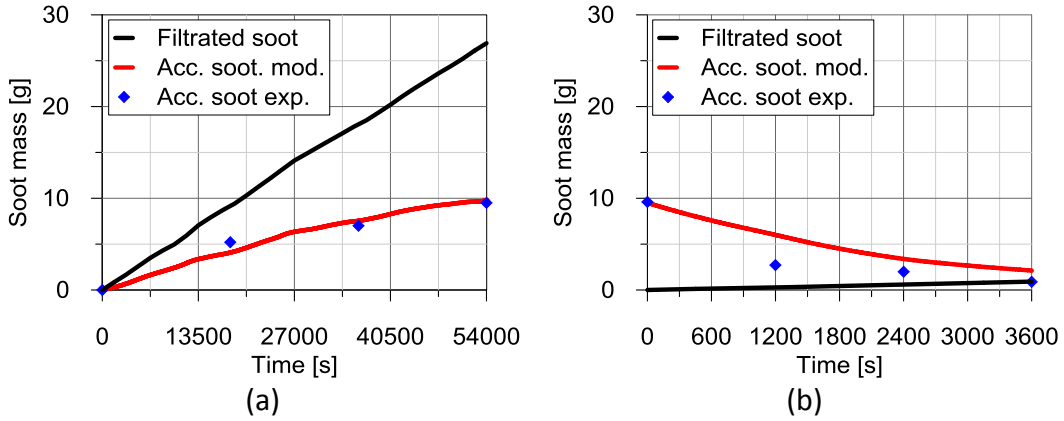

Figure 22. Calibration results for the DPF filtration, regeneration and accumulation for both (a) loading and (b) active regeneration process.

3. Results and discussion

The result section is divided into two subsections. The first one addresses the engine-out results, i.e., without aftertreatment system. This allows to evaluate the potential of the DMDF concept, evidencing its drawbacks and advantages as well as the effect of the truck payload and driving cycles on the results. All the results are referenced with respect to the conventional diesel calibration. Second, the aftertreatment is included to evaluate the performance of the stock DOC in converting the excessive concentration of unburned products. The dominant parameters as well as the effect of payload and driving cycle on the tailpipe emissions are presented. Moreover, the DPF model is also considered to assess the different phenomena as filtration and regeneration during each one of the driving cycles.

3.1. Performance and engine-out emissions

Figure 23 presents the cumulative results for the fuel consumption and the different engine-out contaminants for the WHVC driving cycle and for the three different payloads (0%, 50% and 100%). This payload sweep allows to characterize the parameter dependency with respect to the engine operation. Considering the results of Figure 23(a), it can be concluded that the fuel consumption differences changes at a different ratio for the different payloads (1.396 for the payload ratio of 50%/0% and 1.286 for the 100%/50% truck payload ratio) . It means that, as the payload is increased, the operating conditions are shifted to map zones with higher fuel-to-work conversion efficiencies, proving a more efficient operation. Figure 24 illustrates the operating points inside the efficiency map for the different payloads. As it is shown, the operating points are consistently shifted to higher load conditions as the payload is increased. These zones are prone to deliver higher efficiencies either by the fully premixed combustion at medium load operation or the highly efficient dual-fuel diffusive combustion strategy from medium-to-full load. Therefore, it can be stated that the higher payloads allow to decrease the time usage at low engine load conditions where the efficiency is low due to both high combustion efficiency and friction importance on the brake results. A positive effect with the payload increase is also verified for the unburned hydrocarbon and carbon monoxide emissions. For a payload increase from 50% to 100%, the increase

of the difference in the cumulative values are reduced by a factor higher than 4 compared to the previous step in the case of the HC emissions. This can be easily correlated to the experimental maps and the combustion strategy presented in section 2.3, following the same approach than that used for the brake efficiency analysis.

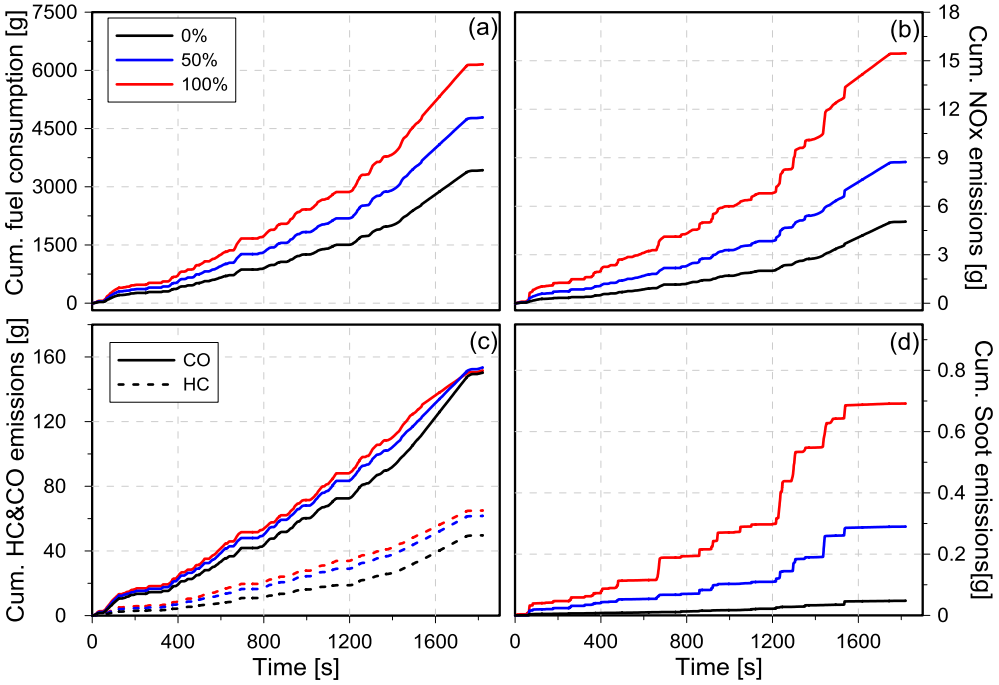

Figure 23. Cumulative results for (a) fuel consumption (b) NOx c) unburned hydrocarbon and carbon monoxide and (d) soot emissions for the WHVC driving cycle considering three different payload levels (0%, 50% and 100%).

As previously discussed, once the engine load is increased towards full load operation, the use of premixed combustion starts to be impracticable due to the mechanical limitations. Therefore, the combustion process is modified targeting lower gasoline fractions and higher diffusive combustion. This enhances the oxidation mechanism of the hydrocarbons and decrease the amount of fuel that enters into the piston gaps during the compression stroke. In this sense, the use of high payloads requires high engine load conditions which avoid the use of the bottom part of the calibration map, reducing the penalization in terms of HC. This conclusion can be also extended to the CO emissions. Nonetheless, the differences are less perceptible since the higher values of this pollutant are restricted to a narrow zone in the bottom part of the calibration map. By contrast, NOx and soot emissions are penalized as the payload is increased, as shown in Figure 23(c) and Figure 23(d). Previous studies demonstrated that the high to full load conditions are a challenging scenario for the DMDF combustion as different limitations coexists (pressure gradient, air management system, etc.). In this sense, the NOx and soot values are relaxed to provide the same power output than that from the original calibration. Consequently, as the payload is increased, the truck operates a higher time fraction at these engine loads, meaning that the production both emissions is enhanced.

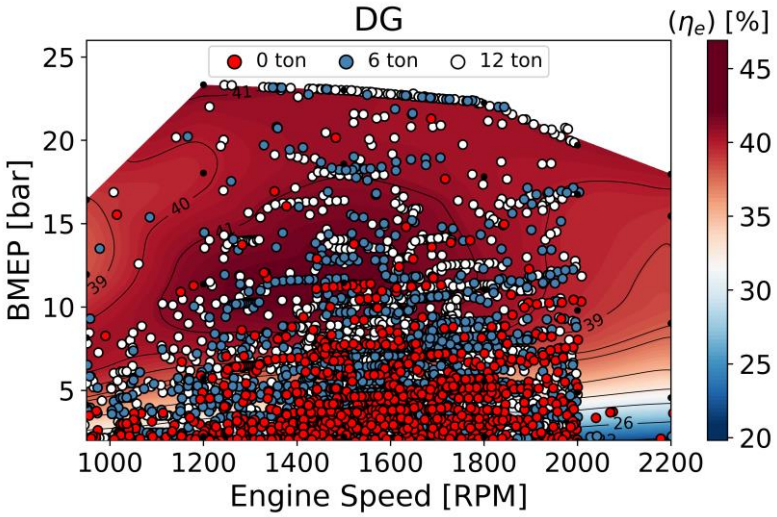

Figure 24. Operating points distribution inside the brake efficiency map for different truck payloads in the world harmonized vehicle cycle.

Once the effect of the different payloads is discussed, the evaluation of the combined effect of the different driving cycles and the payloads on the truck performance is assessed. Figure 25 to Figure 28 illustrate the results for each one of the payloads and driving cycles. The results are presented in percentage differences compared to those that are obtained considering the original conventional diesel combustion calibration map. It should be remarked that the color scheme as well as the size of the circle are representative of the differences obtained during the comparison. Moreover, these results are compared to the normative references. Whenever the DMDF concept is EUVI compliant for the parameter in evaluation, the text color is modified to green, and a black border is added to the circle.

Figure 25 depicts the fuel consumption variation for the different driving cycle and payload. As it is shown, the effect of the payload, previously discussed, can be extended for most of the driving cycles. Nonetheless, the urban case has a minimum point at 50% of the engine load. This driving cycle has a lower velocity variation, which means that the operating point distribution should be more uniform than the remaining driving cycles. In this sense, it is expected that once these operating points approach the medium load of the engine, the higher efficiency will be achieved. It is suggested that this scenario is achieved with 50% of payload. Once the truck payload is increased, the operating points are shifted towards high load, where the efficiency values are decreased because of the higher combustion durations from the diffusive combustion. It should be remarked that the highest fuel consumption penalization rounds 2.8% compared to the CDC combustion at 0% of payload, which can be attributed to the lower efficiency of the DMDF concept due to the combustion efficiency losses at low load. It is also interesting to note that the driving cycles with highway phases are the ones that deliver lower differences compared to the CDC calibration. This suggests that the combustion concept should be better fitted to long haul distribution than the urban usage, where solutions as hybridization are much more attractive.

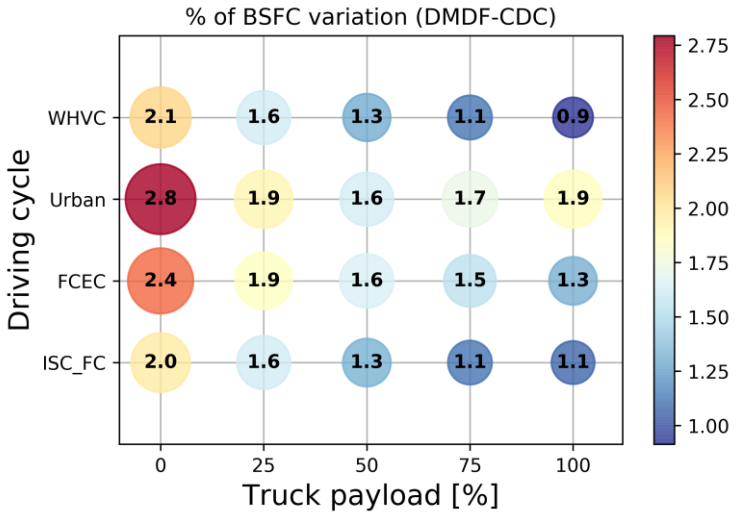

Figure 25. Percentage of driving cycle averaged brake fuel consumption difference between the Dual-Mode Dual-Fuel and the conventional diesel combustion modes.

In spite of the interesting results of the fuel consumption, the most significant benefits are achieved in terms of NOx and soot emissions as depicted in Figure 26. Considering the results of Figure 26 (a), it can be concluded that the proposed combustion concept is able to deliver at least, a reduction of 87 % of the NOx emissions for the test matrix evaluated. Moreover, the assessment of the NOx emissions at normative conditions, i.e., at 50% of payload allows to conclude that the use of the DMDF combustion concept allows to realize engine-out NOx EUVI compliant independently on the driving cycle evaluated. This means that the complex aftertreatment system for NOx reduction could be removed from the powertrain, simplifying and reducing the vehicle costs. It is interesting to note that most of the driving cycles can provide EUVI NOx emissions for the complete payload sweep. However, the WHVC restricts the extension of this assertive, since payloads higher than 50% exceed the normative limits due to the higher number of operating conditions that achieve the high engine loads, where the NOx emission is relaxed. These differences between the WHVC and the ISCs cycles relies on the fact that the ISCs normative includes relaxation factors of 1.5 for each one of the emissions.

Contrarily to the NOx emissions, the DMDF concept cannot realize soot emissions lower than 0.01 g/kWh for the normative driving cycle condition. As previously discussed, the strategy modification from fully premixed to dual-fuel diffusive combustion required a relaxation of the soot limit to fulfill the NOx emissions while achieving brake high efficiency results. This leads to a wider zone map outside of the 0.01 g/kWh limits for soot than the non-compliant EUVI NOx, as it can be seen in the maps from section 2.3. In this sense, despite achieving reductions of 57%, the proposed calibration cannot accomplish soot levels lower than 0.01 g/kWh at normative conditions, thus requiring a dedicated aftertreatment system to deal with this pollutant. It should be remarked that the lower mass produced during the truck operation would require a smaller DPF than that used for the conventional diesel truck. As the truck payload is increased, the benefits in terms of soot emissions are less significant due to the increase of the high engine load zone usage.

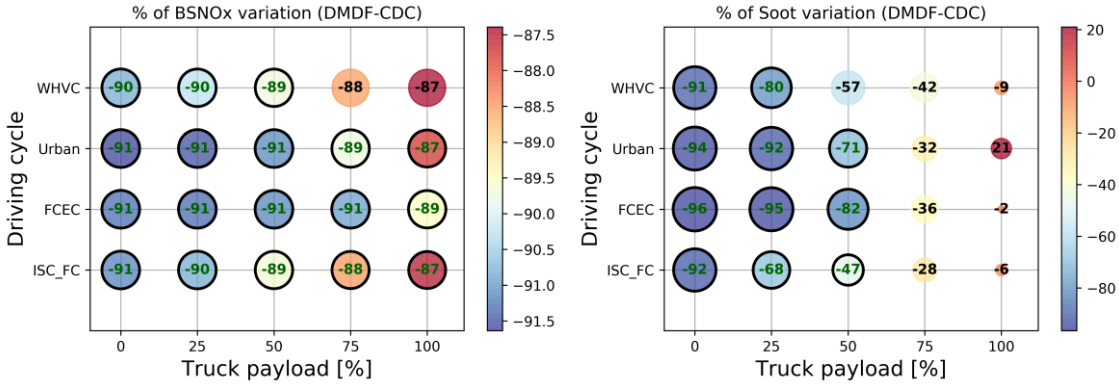

Figure 26. Percentage of difference for (a) NOx and (b) soot driving cycle averaged emission between the Dual-Mode Dual-Fuel and the conventional diesel combustion modes.

Figure 27 presents the results obtained for unburned hydrocarbon and carbon monoxide emissions. As it can be seen, a significant penalization is verified for both emissions independently on the payload and driving cycle evaluated. As previously reported in the literature, these contaminants are one of the most critical drawbacks of the low temperature combustion [62]. Nonetheless, it should be observed that the DMDF combustion is compared to the conventional diesel combustion, which can provide extremely lower CO and HC levels due to the diffusive combustion. Therefore, despite the higher percentage differences, in some cases, the combustion model can still be able to provide values lower than the normative, e.g., CO emissions for the ISC_FC at full payload. It is also interesting to note that Figure 27 (a) has an inverse trend according to the payload than the remaining graphs. This is justified by the higher HC emissions that can be found at low load for the CDC combustion compared to the levels that are produced at high load operation.

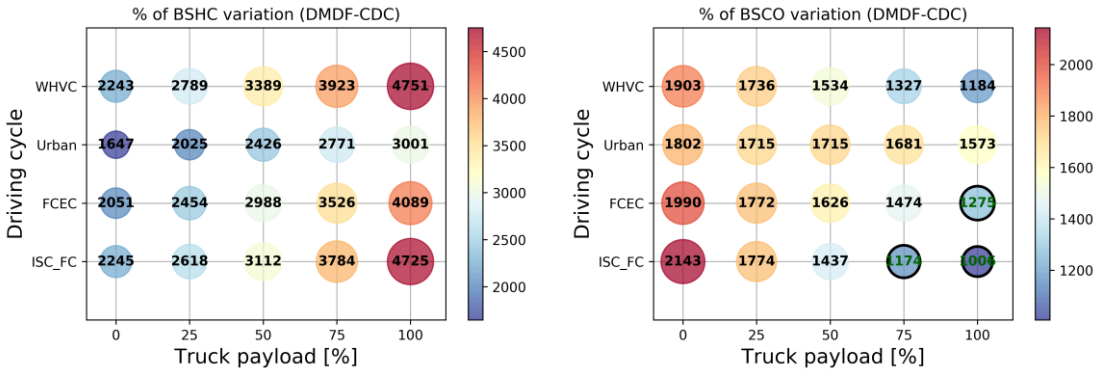

Figure 27. Percentage of difference for (a) unburned hydrocarbon and (b) carbon monoxide driving cycle averaged emission difference between the Dual-Mode Dual-Fuel and the conventional diesel combustion modes.

The results of both emissions shown in Figure 27 are a direct reflect of the lower efficiency of the combustion process. This means that the efficiency results are directly impacted by these pollutant levels. Figure 28 depicts the combustion efficiency results considering both pollutants plus the H_2 emissions (calculated according to the methodology proposed by [63]) to demonstrate the impact on the brake efficiency reduction. As it can be seen, the combustion inefficiency can be as higher as 2.4% compared to the diesel operation, which represents more than 80% of the penalization

on fuel consumption discussed in Figure 25. It is clear that the reduction of this pollutants to similar levels than those from CDC combustion is not feasible due to the nature of the premixed combustion process. Nonetheless, it is suggested that strategies to improve the combustion efficiency or reuse the exhaust gases to recuperate the species with energy availability (CO, HC, H_2) could decrease the penalization on fuel consumption compared to the CDC.

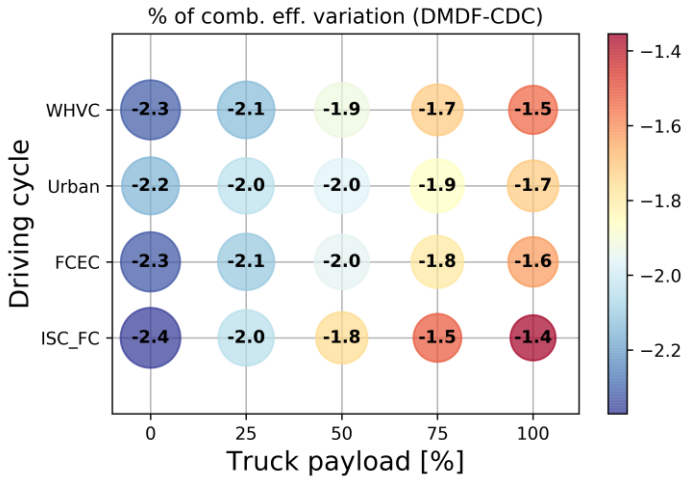

Figure 28. Percentage of driving cycle averaged combustion efficiency difference between the Dual-Mode Dual-Fuel and the conventional diesel combustion modes.

From the previous analysis, it can be concluded that the vehicle powertrain should provide paths to reduce soot, HC and CO emissions. While soot seems to be a less critical point, HC and CO are order of magnitudes higher than those verified in the conventional diesel operation. Moreover, the exhaust gas temperature is expected to be lower because of the lower in-cylinder temperature from the premixed combustion. Therefore, the performance of the stock after treatment system for these pollutants (DOC +DPF) should be evaluated to assess the impact of the DMDF combustion on these devices and feasibility of having a EUVI compliant vehicle with the conventional ATS system for both WHVC and ISCs driving cycles.

3.2. After treatment system analysis

As discussed in the methodology section, the ATS analysis is divided into two different stages. First, the diesel oxidation catalyst is evaluated for the proposed test matrix of payloads and driving cycles. Once the simulation is finished, the results are used as boundary conditions for an in-house DPF model.

Figure 28 depicts the DOC behavior in terms of conversion efficiency along the WHVC driving cycle at normative conditions (50% of truck payload). As it can be seen, the conversion efficiency is directly related to the vehicle velocity and the duration of the zero velocity stages. As higher is the vehicle velocity, higher should be the temperatures and mass flows through the exhaust line, delivering enough energy to the oxidation reactions. Moreover, from Figure 28 it can be concluded that the most critical DOC operation is verified at the beginning of the driving cycle, where the temperature is lower, and the high frequency of zero velocity points cools-down the DOC walls [64]. As the driving cycle progresses towards the rural and highway phases, the efficiency in consistently increased. The CO emissions are maintained near 100% conversion

efficiency values while the HC conversion rarely falls under light-off conditions. It should be also highlighted the long period to achieve light-off in the early phases of the driving cycle, which can consistently increase the tailpipe HC emissions.

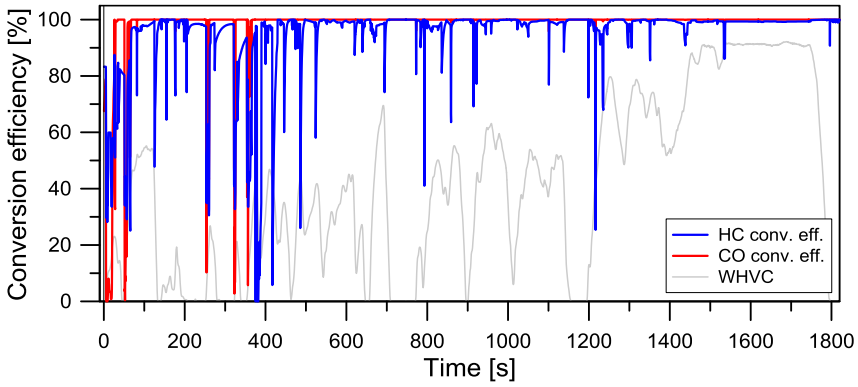

Figure 28. DOC unburned hydrocarbon and carbon monoxide conversion efficiency for the WHVC driving cycle at 50% of payload.

It is expected that the truck payload should also have a significant influence on the conversion efficiency results since this parameter modifies the operating condition distribution inside the engine map. In this sense, Figure 28 (a) demonstrates the effect of the payload on the unburned hydrocarbon conversion efficiency. The analysis on CO emissions is omitted for the sake of brevity as it demonstrated to be less critical in terms of conversion efficiency. Figure 28 (a) presents a kernel density estimation (kde) plot of the HC conversion efficiency for three different payloads. As it is shown, the empty truck has a broader spectrum of conversion efficiency with significant conversion efficiencies from 94%. However, as the payload is increased to 50% and then to 100%, the range is narrowed to values from 97% to 100%. In addition, the kernel density is higher addressing more data points, which can be inferred by their higher peak. The improvement of the conversion efficiency with the payload can be directly correlated with the different boundary conditions at the DOC inlet. Based on this, the effect of the payload on the temperature distribution was also assessed, being depicted in Figure 29 (b). The same kernel density estimation approach was used, allowing to identify the relevant kernels of the temperature distribution as well as providing a database for probability density function (PDFs) construction. The figure analysis demonstrates a direct dependence of the temperature values with the truck payload. This means that as the payload is increased and the operating points are shifted to higher engine loads, the engine out temperature are higher, providing benefits in terms of HC conversion efficiency. This conclusion can be extended also to the CO emissions given its dependency on the temperature.

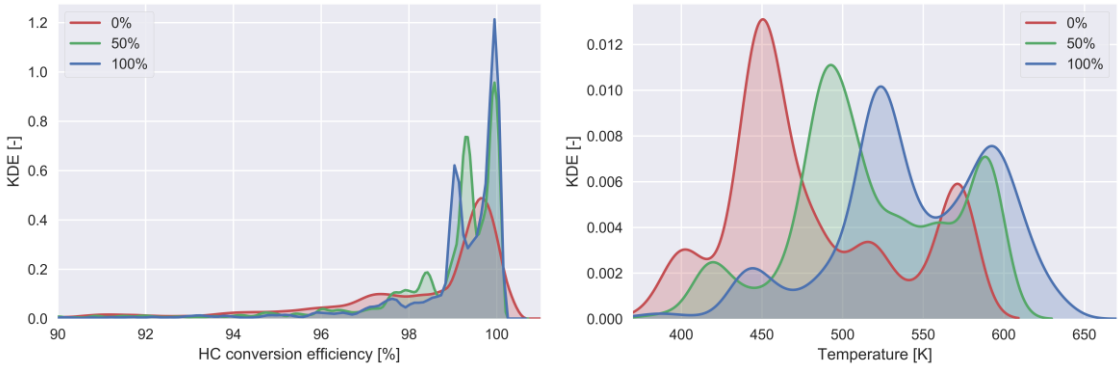

Figure 29. Kernel density estimation profiles for both (a) unburned hydrocarbon conversion efficiency and (b) DOC inlet temperature at the WHVC for three different payloads (0%, 50% and 100%).

The overview of the ATS performance for the complete test matrix is presented in Figure 30 for both HC (a) and CO (b). The same indication is presented to different EUVI compliant conditions (green font and black border). Before the discussion, it should be remarked that all the results are referenced to the CDC engine-out driving cycle average results, which could provide different trends than those previously observed in the engine-out section. With that in mind, the different results according to the payload and driving cycle can be discussed. Figure 30 (a) presents the difference of the HC emissions compared to the levels of the conventional diesel combustion. In which regards the WHVC, a minimum difference is achieved at 50% of payload (normative condition). At the same time, this is the first payload that starts to be EUVI compliant for HC emissions. Such improvement with respect to the payload was previously addressed, indicating that the temperature increase with the higher engine loads should be a dominant factor on the conversion efficiency. From 50%, the difference compared to the diesel combustion starts to increase again, which is a direct result of the extremely low levels of HC produced by the conventional diffusive diesel combustion. In this sense, it can be concluded that the DMDF combustion mode still presents at least 31% more HC emissions at the WHVC driving cycle. Nonetheless, this conclusion cannot be extended to the remaining driving cycles. These driving conditions can deliver more consistent reductions compared to the CDC operation, once they present shorter zero velocity times and higher absolute velocity values than those presented in the critical part of the WHVC (urban phase). Therefore, with exception of the fuel consumption driving cycle (FCEC), reductions up to 93% are achieved compared to the CDC reference, achieving the limits imposed by the EUVI for this pollutant, independently on the payload.

Figure 30 (b) presents the DOC performance in converting the CO emissions. As discussed at the beginning of the section, CO emissions are easily converted in the DOC since the energy of activation of its oxidation reaction is significantly lower than the ones required to oxidize the lower reactivity hydrocarbons in the exhaust gases. Therefore, even in low truck payload conditions, the DOC can convert most of the carbon monoxide, delivering EUVI CO compliant emissions independently on the driving cycle and payload. Moreover, all the assessed conditions presented reductions compared to the CDC engine-out CO emissions. The lower differences are experienced at low truck payloads and as a consequence of the lower DOC inlet temperatures.

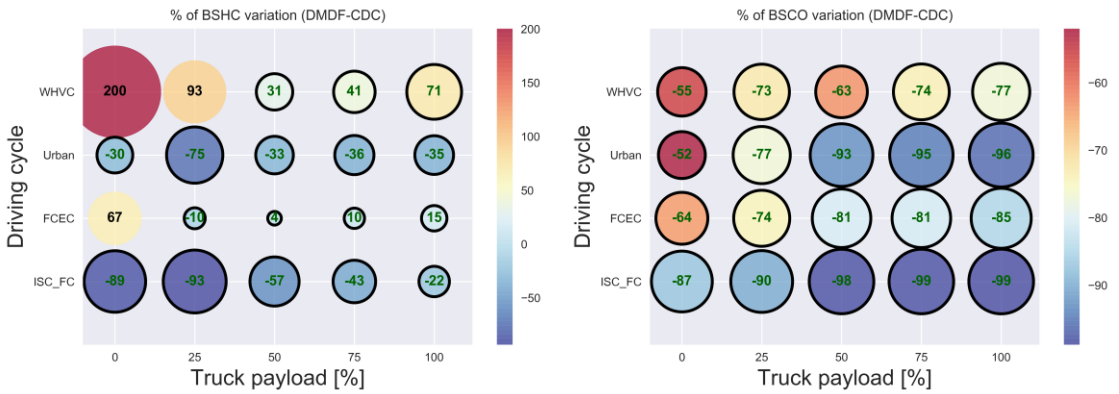

(a) (b)

Figure 30. Percentage of difference for (a) unburned hydrocarbon and (b) carbon monoxide driving cycle averaged emission difference between the Dual-Mode Dual-Fuel and the conventional diesel combustion modes.

Figure 31 summarizes the impact of the DOC usage on both HC and CO emissions for the payloads and driving cycle evaluated. The blue circles represent the engine-out emissions while the green ones are the driving cycle average values after the DOC (tailpipe emissions). Moreover, the black dashed line stands as the EUVI limits for each one of the pollutants. The first interesting observation is the linear behavior that the average HC emission presents with respect to the truck payload, mainly for the first three cycles. By contrast, this behavior is not translated at the DOC outlet, where at the WHVC, for example, the decrease of the payload provides an exponential increase in the HC emissions for the cases where the normative is not fulfilled. This behavior relies on the kinectics present in the DOC, which have a strong exponential dependency on the temperature. This last was demonstrated to be directly impacted by the truck payload. Once the EUVI limits are achieved, the variation is mitigated as the values are as lower as 0.13 g/kWh. It is also interesting to remark that despite the considerable variation on the velocity profiles of each driving cycle, the engine-out average emissions present small variations on their absolute value.

The same analysis can be extended to the carbon monoxide emissions as presented in Figure 31 (b). As previously presented, this emission can be fully addressed by the DOC, independently on the driving cycle and payload investigated. As shown in the graph, the CO emissions have a higher dispersion among the driving cycles and an opposite trend compared to the HC values. While the HC emission are higher for the ISC_FC (full cycle), the CO emissions present its minimal value for this condition, independently on the payload. This is a consequence of the emission maps presented in section 2.3, i.e., the combustion mode that is used in each region. The fully premixed combustion provides the highest HC values at medium load while the CO are less impacted by this combustion strategy. The CO emission is more significant at low load conditions, where the in-cylinder temperature does not provide enough energy to the complete oxidation in the end of the reaction path, increasing the CO concentration. Nonetheless, as the engine load is increase towards medium load, this condition is fulfilled, decreasing the concentration of carbon monoxide. This decoupled mechanism between HC and CO emissions is the main reason to have the significant differences on the calibration maps and, consequently, on the driving cycle results.

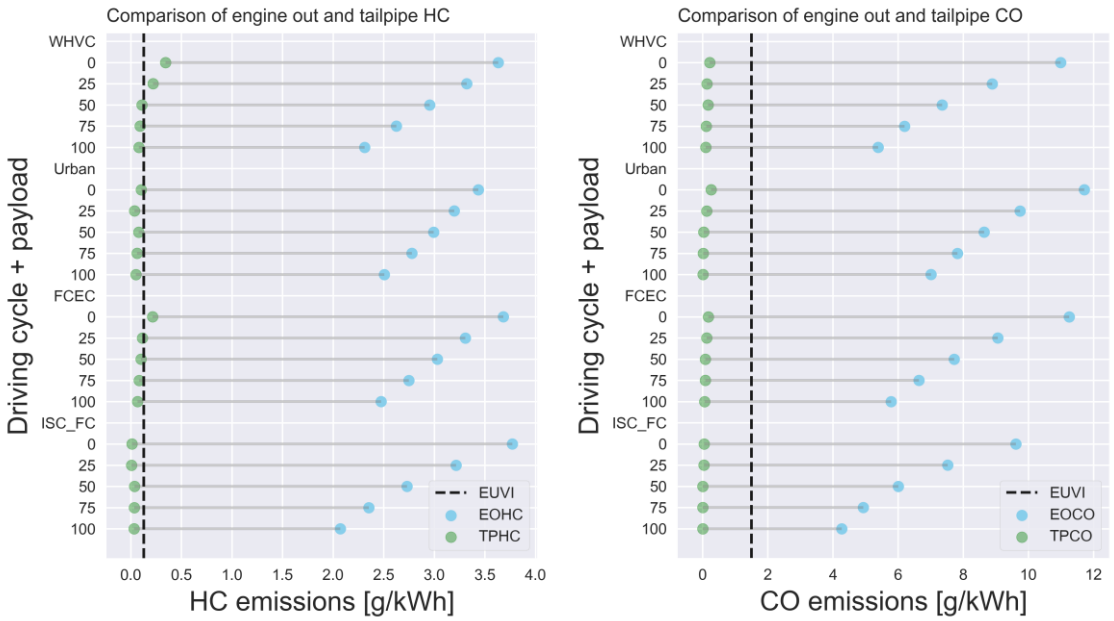

(a) (b)

Figure 31. Comparison of both engine-out and tailpipe emissions for both (a) unburned hydrocarbons and (b) carbon monoxide for the different payloads and driving cycles. The vertical dashed line stands for the EUVI limits for each emission.

From this analysis, it can be inferred that the stock diesel oxidation catalyst is able to deliver tailpipe normative emissions considering both WHVC and in-service conformity driving cycles, even in the case of having the considerable higher concentrations of unburned products at engine-out. It is interesting to note that once these species are converted, they deliver a significant amount of energy, increasing the temperature of the DOC, enhancing the oxidation process. It is suggested that this is one of the main justifications to achieve the high conversion efficiencies once the DOC is properly operating. This temperature increase on steady-state conditions was reported in previous works. Detailed quantitative analysis and discussion can be found at [41].

Among the different engine-out pollutants, the proposed evaluation demonstrated that NOx can be mitigated by the combustion process while HC and CO can be dealt by the stock DOC system. Nonetheless, it was concluded that the DMDF combustion exceeds the soot limits proposed by the EUVI even in the case of considering only the fraction of the particle matter than can be measured by the AVL 415S smoke meter. In this sense, the performance of the current DPF system is suggested. Since the WHVC was the unique driving cycle that did not fulfill the soot EUVI limit in which regards the particle matter of 0.01 g/kWh, this analysis will be focused only on the DPF performance for this driving cycle.

Figure 32 presents the cumulative soot emissions dependency with the truck payload considering the WHVC. As it was previously evidenced, the increase of the truck payload pushes the operating conditions to higher loads, at higher power conditions to fulfill the energy requirements of the driving cycle. Consequently, the soot mass is penalized since these operating conditions are prone to produce significant quantities of soot due to the diffusive combustion on environments with low oxygen concentration. The results from Figure 34 allow also to conclude that the more than half of the soot mass is produced in the highway phase of the driving cycle, independently on the payload evaluated. It

should be remarked that this is the total soot mass produced along the driving cycle and not a representation of the accumulated soot in the DPF.

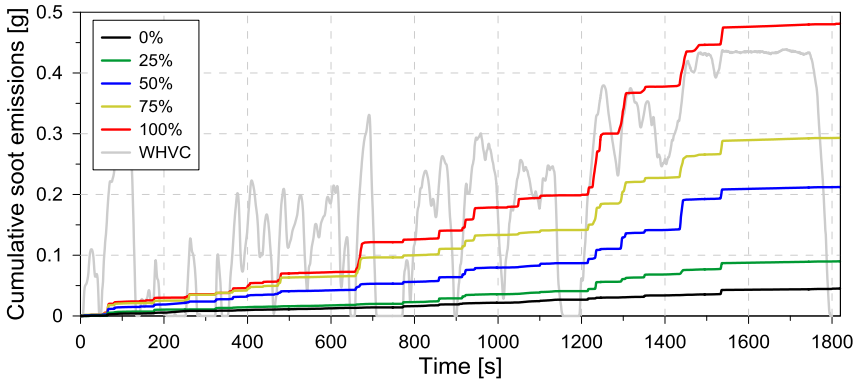

Figure 32. Soot mass produced during the WHVC driving cycle for the different truck payloads.

Differently from the DOC and SCR after treatment devices, the DPF operation relies on the filtration of the exhaust gases, retaining the solid particles, i.e., it does not use directly chemical reactions to reduce the quantity of pollutants at the exhaust [65].Therefore, one of the most important process that should be considered is the soot filtration, which determines the soot that can be trapped in the DPF. Generally, the soot filtration efficiencies are as high as 99% [66]This level is increased as the soot mass trapped increased. Figure 33 presents the results of the filtrated soot mass with respect to the different payloads. As it is depicted, the filtrated mass is similar to the produced mass by the combustion process, demonstrating that the DPF is able to deal with the soot produced by the combustion concept.

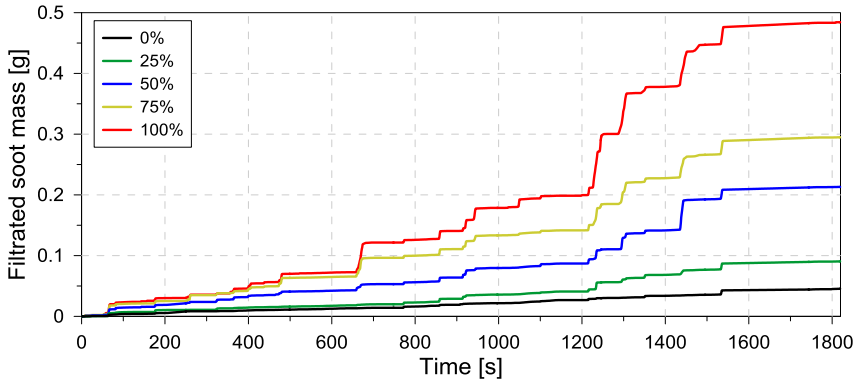

Figure 33. Filtrated soot mass by the DPF during the WHVC driving cycle for the different truck payloads.

Nonetheless, this last effect implies higher pumping losses due to the pressure drop along the DPF, which can reduce the engine efficiency and modify the operating conditions of the air management system. Therefore, the total pressure drop due to the increase of the PF load was assessed and is presented in Figure 34. It should be stated that this pressure drop is a sum of different losses that take place on the monolith as the inertial and friction pressure losses. The first is highly impacted by the total mass flow whilst the second is related to the flow area through the monolith[67]. These dependencies are reflected on the monolith pressure drop presented in Figure 34, which increases with both payload and filtrated soot mass. However, even in the worst scenario, the pressure drop was as higher as 30 mbar. These levels are similar to those of partially loaded filters and are not problematic in which regards the engine operation

and its consequent efficiency degradation [68]. Therefore, it can be stated that the original DPF is oversized for the DMDF combustion concept. This means that specific studies should be performed aiming to determine a new DPF size that could provide cost savings while dealing with the levels of soot mass without impacting the pressure drop.

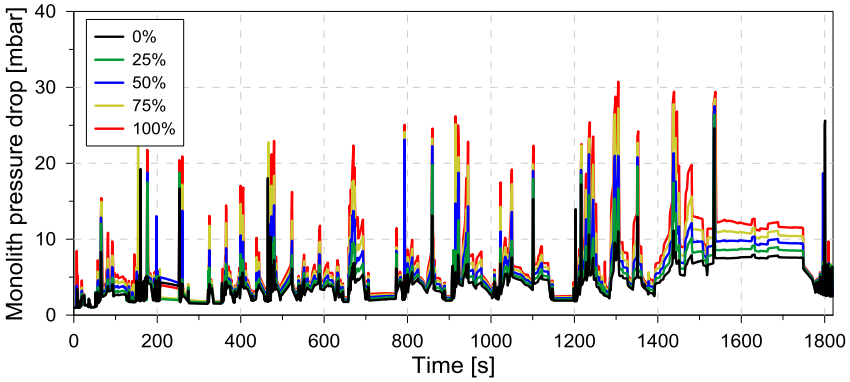

Figure 34. Monolith pressure drop at the DPF during the WHVC driving cycle for the different truck payloads.

Finally, the regeneration of the DPF is assessed. In this case, both passive regeneration by means of NO_2 [69] or O_2 [70] are considered. It should be stressed that the passive regeneration by O_2 herein discussed is a consequence of the high temperature at the exhaust gases after the DOC from the conversion of HC and CO. This differs from the high temperature active regeneration enabled by an additional fuel injection. The results presented in Figure 35 demonstrates that the DPF regeneration is appreciable only at the highway phase of the WHVC. In this phase, both NO_2 concentration and the exhaust temperature is increased. Nonetheless, previous analysis suggests that the soot regeneration is dominated by the O_2 oxidation path, since even in high load operation, the NO_2 concentration does not exceeds 150 ppm.

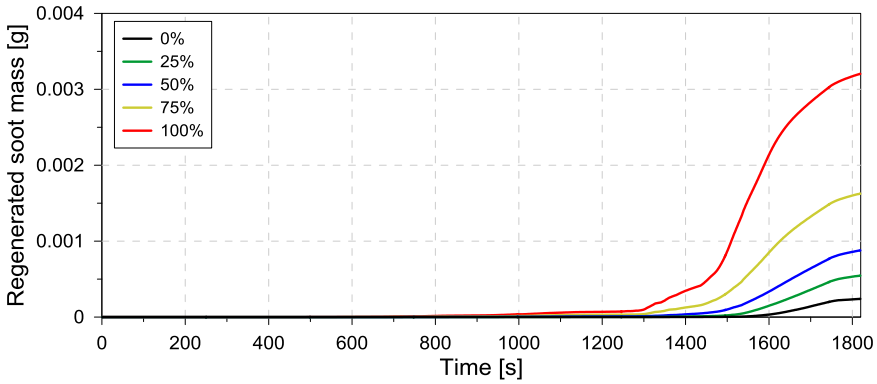

Figure 35. Regenerated soot mass by both passive and high temperature oxidation at the DPF during the WHVC driving cycle for the different truck payloads.

4. Conclusions

This paper presented the potential of using the Dual-Mode Dual-Fuel combustion concept on normative and real life applications comprehending performance, engine-out and tailpipe assessment. To do this, a rigorous methodology was applied following several calibration and validation steps for the truck and the aftertreatment system to guarantee the results reliability. After that, the validated model was submitted to

different driving cycles: WHVC (normative), In-service conformity test, real life urban and fuel consumption evaluation cycle with different truck payloads. First, the performance and engine-out emissions were assessed to provide an overview of the benefits and drawbacks of the concept compared to the original CDC calibration. The most significant remarks are:

- There is a small fuel consumption penalization by using the DMDF combustion, independently on the driving cycle and payload investigation due to the efficiency decrease at high load and low engine speed operation.
- The use of the DMDF combustion allows to fulfill EUVI NOx for the normative conditions (WHVC and 50% of payload), allowing to remove the SCR system and, consequently, to reduce both operational and vehicle cost.
- Both unburned hydrocarbons and carbon monoxide are increased due to the premixed combustion, exceeding by far the EUVI normative.
- Soot emissions are significantly reduced, but not to levels that allows to provide engine-out values comparable to the EUVI limits.

Given the last two considerations, a dedicated evaluation of the engine stock aftertreatment system for HC, CO and soot was performed, aiming to assess their potential on providing EUVI compliant emissions and the consequent impact of the DMDF concept on their performance. From this analysis, it can be concluded that:

- The conventional oxidation catalyst can reduce the HC and CO levels to those of EUVI normative from 50% of payload. Lower payloads than 50% implies low DOC inlet temperatures, impairing the conversion efficiency for HC in an exponential way. Carbon monoxide is fully addressed by the DOC due to its high reactivity.
- The particulate filter can deal with the total soot emissions produced during the driving cycle, independently on the payload. The maximum values of filtrated soot imply low monolith pressure drop which are not critical for the engine operation. Nonetheless, it was demonstrated that the passive regeneration is not able to reduce the soot mass inside the particulate filter suggesting that an active regeneration should be investigated to guarantee the DPF cleaning.

In this sense, it can be concluded that the DMDF combustion concept can be an alternative to reduce the costs associate with aftertreatment system by both SCR removal and DPF resizing while dealing with the unburned products with the conventional oxidation catalyst. Nonetheless, this is accomplished by penalizing the fuel consumption values by as far as 2.4%, depending on the payload investigated. Generally, the DMDF presents a better performance in complete driving cycle with high payloads, suggesting that this concept is most suitable for long haul application that highly urban scenarios where different solutions as powertrain hybridization can have greater potential.

Acknowledgments

The authors thanks ARAMCO Overseas Company and VOLVO Group Trucks Technology for supporting this research. The authors acknowledge FEDER and Spanish Ministerio de Economía y Competitividad for partially supporting this research through TRANCO project (TRA2017-87694-R). The authors also acknowledge the Universitat Politècnica de València for partially supporting this research through Convocatoria de ayudas a Primeros Proyectos de Investigación (SP20180148). The author R. Sari acknowledges the financial support from the Spanish ministry of science innovation and universities under the grant ‘‘Ayudas para contratos predoctorales para la formación de doctores” (PRE2018-085043).

References

[1] COMMISSION REGULATION (EU) No 136/2014. Amending Directive 2007/46/EC of the European Parliament and of the Council, Commission Regulation (EC) No 692/2008 as regards emissions from light passenger and commercial vehicles (Euro 5 and Euro 6) and Commission Regulation (EU) No 582/2011 as regards emissions from heavy duty vehicles (Euro VI). 11 February 2014.

[2] Rao G, Kaleemuddin S. Development of variable timing fuel injection cam for effective abatement of diesel engine emissions. Applied Energy, Volume 88, Issue 8, 2011, Pages 2653-2662.

[3] Agarwal A. K., Dhar A., Gupta J. G., Kim W, Lee C, Park S. Effect of fuel injection pressure and injection timing on spray characteristics and particulate size–number distribution in a biodiesel fuelled common rail direct injection diesel engine. Applied Energy, Volume 130, 2014, Pages 212-221, ISSN 0306-2619.

[4] Prasad B.V.V.S.U., Sharma C.S., Anand T.N.C., Ravikrishna R.V. High swirl-inducing piston bowls in small diesel engines for emission reduction, Applied Energy, Volume 88, Issue 7, 2011, Pages 2355-2367.

[5] Russell A, Epling W S. Diesel Oxidation Catalysts. Catalysis Reviews: Science and Engineering. Volume 53, 2011, Pages 337-423

[6] Serrano JR, Bermudez V, Piqueras P, Angiolini E. Application of Pre-DPF Water Injection Technique for Pressure Drop Limitation. SAE Technical Paper 2015-01-0985. https://doi.org/10.4271/2015-01-0985.

[7] Ettireddy PR, Kotrba A, Spinks T, Boningari T, Smirniotis P. Development of Low Temperature Selective Catalytic Reduction (SCR) Catalysts for Future Emissions Regulations. SAE Technical Paper 2014-01-1520. https://doi.org/10.4271/2014-01-1520.

[8] Henry C, Currier N, Ottinger N, Yezerets A. Decoupling the Interactions of Hydrocarbons and Oxides of Nitrogen Over Diesel Oxidation Catalysts. SAE Technical Paper 2011-01-1137. doi:10.4271/2011-01-1137.

[9] Zhang J., Wong V. W., Shuai S., Chen Y., Sappok A. Quantitative estimation of the impact of ash accumulation on diesel particulate filter related fuel penalty for a typical modern on-road heavy-duty diesel engine. Applied Energy, Volume 229, 2018, Pages 1010-1023, ISSN 0306-2619.

[10] Payri, F., Arnau, F.J., Piqueras, P., and Ruiz, M.J. Lumped Approach for Flow-Through and Wall-Flow Monolithic Reactors Modelling for Real-Time Automotive Applications. SAE Technical Paper 2018-01-0954, 2018, doi:10.4271/2018-01-0954.

[11] Liang Z., Ma X., Lin H., Tang Y. The energy consumption and environmental impacts of SCR technology in China, Applied Energy, Volume 88, Issue 4, 2011, Pages 1120-1129, ISSN 0306-2619.
[12] Pastor J. V., García A., Micó C, Lewiski F. An optical investigation of Fischer-Tropsch diesel and Oxymethylene dimethyl ether impact on combustion process for CI engines. Applied Energy, Volume 260, 2020, 114238, ISSN 0306-2619.
[13] Pan J, Wei H, Shu G, Chen Z, Zhao P. The role of low temperature chemistry in combustion mode development under elevated pressures. Combustion and Flame, Volume 174, 2016, Pages 179-193.
[14] Lawler B, Splitter D, Szybist J, Kaul B. Thermally Stratified Compression Ignition: A new advanced low temperature combustion mode with load flexibility. Applied Energy, Volume 189, 2017, Pages 122-132, ISSN 0306-2619.
[15] Pachiannan T., ZhongW, RajkumarS , He Z , Leng X, Wang Q. A literature review of fuel effects on performance and emission characteristics of low-temperature combustion strategies. Applied Energy, Volume 251, 2019, 113380, ISSN 0306-2619.
[16] Krishnamoorthi M., Malayalamurthi R., He Z, Kandasamy S. A review on low temperature combustion engines: Performance, combustion and emission characteristics. Renewable and Sustainable Energy Reviews, Volume 116, 2019, 109404, ISSN 1364-0321.
[17] Javier López J., García-Oliver J.M., García A., Domenech V. Gasoline effects on spray characteristics, mixing and auto-ignition processes in a CI engine under Partially Premixed Combustion conditions. Applied Thermal Engineering, Volume 70, Issue 1, 2014, Pages 996-1006, ISSN 1359-4311.
[18] Hyvönen J., Haraldsson G., Johansson, B. Operating range in a Multi Cylinder HCCI engine using Variable Compression Ratio. SAE Technical Paper 2003-01-1829, 2003, https://doi.org/10.4271/2003-01-1829.
[19] Komninos N.P., Rakopoulos C.D. Heat transfer in hcci phenomenological simulation models: A review. Applied Energy, Volume 181, 2016, Pages 179-209, ISSN 0306-2619.
[20] Yousefi A, Gharehghani A, Birouk M. Comparison study on combustion characteristics and emissions of a homogeneous charge compression ignition (HCCI) engine with and without pre-combustion chamber. Energy Conversion and Management, Vol. 100, pp. 232-241, 2015.
[21] Martins, M., Fischer, I., Gusberti, F., Sari, R. et al., "HCCI of Wet Ethanol on a Dedicated Cylinder of a Diesel Engine," SAE Technical Paper 2017-01-0733, 2017, https://doi.org/10.4271/2017-01-0733.
[22] Hunicz J, Mikulski M, Geca M, Rybak A. An applicable approach to mitigate pressure rise rate in an HCCI engine with negative valve overlap, Applied Energy, Volume 257, 2020, 114018, ISSN 0306-2619.
[23] Kokjohn S L, Hanson R M, Splitter D A, Reitz R D. Fuel reactivity controlled compression ignition (RCCI): a pathway to controlled high-efficiency clean combustion, International Journal of Engine Research, 2011. Volume 12, June 2011, Pages 209-226.
[24] Benajes J, Molina S, García A, Monsalve-Serrano J. Effects of direct injection timing and blending ratio on RCCI combustion with different low reactivity fuels.

Energy Conversion and Management, Volume 99, 2015, Pages 193-209, ISSN 0196-8904.

[25] Benajes J, García A., Monsalve-Serrano J, Sari R. Fuel consumption and engine-out emissions estimations of a light-duty engine running in dual-mode RCCI/CDC with different fuels and driving cycles. Energy, Volume 157,2018, Pages 19-30, ISSN 0360-5442.

[26] Olmeda P., García A., Monsalve-Serrano J, Sari R. Experimental investigation on RCCI heat transfer in a light-duty diesel engine with different fuels: Comparison versus conventional diesel combustion. Applied Thermal Engineering, Volume 144, 2018, Pages 424-436, ISSN 1359-4311.

[27] Reitz, R.D., Duraisamy, F. Review of high efficiency and clean reactivity-controlled compression ignition (RCCI) combustion in internal combustion engines. Progress in Energy and Combustion Science. Volume 46, August 2014, pages 12-71

[28] J. Benajes, A. García, J. Monsalve-Serrano, D. Villalta, Benefits of E85 versus gasoline as low reactivity fuel for an automotive diesel engine operating in reactivity controlled compression ignition combustion mode, Energy Convers. Manag. 159 (2018) 85–95.

[29] Benajes J, García A, Monsalve-Serrano J, Villalta D. Exploring the limits of the RCCI combustion concept in a light-duty diesel engine and the influence of the direct-injected fuel properties. Energy Conversion and Management, Volume 157, 2018, Pages 277-287.

[30] García A, Monsalve-Serrano J, Rückert Roso V, Santos Martins M. Evaluating the emissions and performance of two dual-mode RCCI combustion strategies under the World Harmonized Vehicle Cycle (WHVC). Energy Conversion and Management, Volume 149, 1 Oct 2017, Pages 263-274.

[31] Benajes J, García A, Monsalve-Serrano J, Boronat V. Achieving clean and efficient engine operation up to full load by combining optimized RCCI and dual-fuel diesel-gasoline combustion strategies. Energy Conversion and Management, Volume 136, 15 March 2017, Pages 142-151.

[32] Benajes, J., García, A., Monsalve-Serrano, J., Boronat, V. Dual-Fuel Combustion for Future Clean and Efficient Compression Ignition Engines. Appl. Sci. 2017, 7, 36.

[33] Benajes J., García A., Monsalve-Serrano J., Sari R. Clean and efficient dual-fuel combustion using OMEx as high reactivity fuel: Comparison to diesel-gasoline calibration. Energy Conversion and Management, Volume 216, 2020, 112953, ISSN 0196-8904.

[34] García A., Monsalve-Serrano J., Villalta D., Sari R. Fuel sensitivity effects on dual-mode dual-fuel combustion operation for different octane numbers, Energy Conversion and Management, Volume 201, 2019, 112137.

[35] García A., Monsalve-Serrano J., Villalta D., Sari R. Octane number influence on combustion and performance parameters in a Dual-Mode Dual-Fuel engine. Fuel, Volume 258,2019, 116140.

[36] García A., Monsalve-Serrano J., Villalta D., Sari R., Zavaleta V., Gaillard P. Potential of e-Fischer Tropsch diesel and oxymethyl-ether (OMEx) as fuels for the dual-mode dual-fuel concept. Applied Energy, Volume 253, 2019, 113622.

[37] Gong C,Yi L, Zhang Z, Sun J, Liu F. Assessment of ultra-lean burn characteristics for a stratified-charge direct-injection spark-ignition methanol engine under different high compression ratios. Applied Energy, Volume 261,2020,114478, ISSN 0306-2619.

[38] Gong C, Zhang Z, Sun J, Chen Y, Liu F. Computational study of nozzle spray-line distribution effects on stratified mixture formation, combustion and emissions of a high compression ratio DISI methanol engine under lean-burn condition, Energy, Volume 205, 2020, 118080, ISSN 0360-5442.

[39] Gong C, Sun J, Liu F. Numerical study of twin-spark plug arrangement effects on flame, combustion and emissions of a medium compression ratio direct-injection methanol engine. Fuel, Volume 279, 2020, 118427, ISSN 0016-2361.

[40] Benajes J, García A, Monsalve-Serrano J, Sari R. Experimental investigation on the efficiency of a diesel oxidation catalyst in a medium-duty multi-cylinder RCCI engine. Energy Conversion and Management, Volume 176, 15 November 2018, Pages 1-10

[41] García A, Monsalve-Serrano J, Villalta D, Sari R. Performance of a conventional diesel aftertreatment system used in a medium-duty multi-cylinder dual-mode dual-fuel engine. Energy Conversion and Management, Volume 184, 2019, Pages 327-337, ISSN 0196-8904.

[42] Gong C, Lib Z, Yi L, Liu F. Comparative study on combustion and emissions between methanol portinjection engine and methanol direct-injection engine with H2-enriched port-injection under lean-burn conditions. Energy Conversion and Management, Volume 200,2019, ISSN 0196-8904.

[43] Gong C, Li Z, Yi L, Liu F. Experimental investigation of equivalence ratio effects on combustion and emissions characteristics of an H2/methanol dual-injection engine under different spark timings. Fuel, Volume 262, 2020, 116463,ISSN 0016-2361.

[44] Gong C, Li Z, Yi L, Huang K, Liu F. Research on the performance of a hydrogen/methanol dual-injection assisted spark-ignition engine using late-injection strategy for methanol. Fuel, Volume 260, 2020, 116403, ISSN 0016-2361.

[45] Park Y., Bae C. Experimental study on the effects of high/low pressure EGR proportion in a passenger car diesel engine. Applied Energy, Volume 133, 2014, Pages 308-316, ISSN 0306-2619.

[46] Benajes, J., García, A., Pastor, J.M., Monsalve-Serrano, J. Effects of piston bowl geometry on Reactivity Controlled Compression Ignition heat transfer and combustion losses at different engine loads. Energy, Volume 98, March 2016, pages 64-77.

[47] AVL manufacturer manual. Smoke value measurement with the filter-papermethod. Application notes. June 2005 AT1007E, Rev. 02. Web:<https://www.avl.com/documents/10138/885893/Application+Notes >.

[48] García A, Gil A, Monsalve-Serrano J, Sari R. OMEx-diesel blends as high reactivity fuel for ultra-low NOx and soot emissions in the dual-mode dual-fuel combustion strategy. Fuel, Volume 275, 2020, 117898, ISSN 0016-2361.

[49] J. Benajes, J.V. Pastor, A. García, J. Monsalve-Serrano. The potential of RCCI concept to meet EURO VI NOx limitation and ultra-low soot emissions in a heavy-duty engine over the whole engine map. Fuel, 159 (November) (2015), pp. 952-961
[50] Turns S. An introduction to combustion: concepts and applications. McGraw-Hill Series in Mechanical Engineering, second edition, 2000.
[51] Volvo trucks: Volvo FE: Available at< https://www.volvotrucks.com.au/en-au/trucks/volvo-fe.html accessed in 16/04/2020>
[52] Gamma Technologies: Vehicle Driveline and HEV Application Manual. 2018.
[53] Luján J, García A, Monsalve-Serrano J, Martínez-Boggio S. Effectiveness of hybrid powertrains to reduce the fuel consumption and NOx emissions of a Euro 6d-temp diesel engine under real-life driving conditions. Energy Conversion and Management, Volume 199, 2019, 111987, ISSN 0196-8904.
[54] COMMISSION REGULATION (EU) No 582/2011.Implementing and amending Regulation (EC) No 595/2009 of the European Parliament and of the Council with respect to emissions from heavy duty vehicles (Euro VI) and amending Annexes I and III to Directive 2007/46/EC of the European Parliament and of the Council. 25 May 2011
[55] Sampara C, Bissett E, Chmielewski M. Global Kinetics for a Commerical Diesel Oxidation Catalyst with Two Exhaust Hydrocarbons. Industrial Engineering and Chemical Research, Volume 47, 18 December 2008, Pages 311-322.
[56] Sampara C, Bissett E, Chmielewski M, Assanis D. Global Kinetics for Platinum Diesel Oxidation Catalysts. Industrial & Engineering Chemistry Research, Volume 46, 6 October 2007, Pages 7993-8003.
[57] Silvis W. An Algorithm for Calculating the Air/Fuel Ratio from Exhaust Emissions. SAE Technical Paper 970514, 1997.
[58] Gamma Technologies: Optimization Manual. 2018.
[59] Wang Q, Wang B, Yao C, Liu M, Wu T, Wei H, Dou Z. Study on cyclic variability of dual fuel combustion in a methanol fumigated diesel engine. Fuel, Volume 164, 2016, Pages 99-109, ISSN 0016-236.
[60] Macián V., Serrano J.R., Piqueras P., Sanchis E.J. Internal pore diffusion and adsorption impact on the soot oxidation in wall-flow particulate filters. Energy, Volume 179, 2019, Pages 407-421, ISSN 0360-5442.
[61] Payri González, F.; Arnau Martínez, FJ.; Piqueras Cabrera, P.; Ruiz Lucas, MJ. (2018). Lumped Approach for Flow-Through and Wall-Flow Monolithic Reactors Modelling for Real-Time Automotive Applications. SAE Technical Papers. doi:10.4271/2018-01-0954
[62] Pedrozo V B, May I, Lanzanova T D M, Zhao H. Potential of internal EGR and throttled operation for low load extension of ethanol–diesel dual-fuel reactivity controlled compression ignition combustion on a heavy-duty engine. Fuel, Volume 179, 1 September 2016, Pages 391-405
[63] Heywood J B. Internal Combustion Engine Fundamentals. McGraw-Hill, 2018, Second edition.
[64] J. Gao, G. Tian, A. Sorniotti, A.E. Karci, R. Di Palo, Review of thermal management of catalytic converters to decrease engine emissions during cold start

and warm up, Appl. Therm. Eng. 147 (2019) 177–187. doi:10.1016/j.applthermaleng.2018.10.037.
[65] Yang, S., Deng, C., Gao, Y., & He, Y. Diesel particulate filter design simulation: A review. Advances in Mechanical Engineering, Volume 8, 2016, https://doi.org/10.1177/1687814016637328.
[66] Serrano J, Climent H, Piqueras P, Angiolini E. Filtration modelling in wall-flow particulate filters of low soot penetration thickness. Energy, Volume 112, 2016, Pages 883-898, ISSN 0360-5442.
[67] Payri F., Broatch A., Serrano J.R., Piqueras P. Experimental–theoretical methodology for determination of inertial pressure drop distribution and pore structure properties in wall-flow diesel particulate filters (DPFs). Energy, Volume 36, Issue 12, 2011, Pages 6731-6744, ISSN 0360-5442.
[68] Bermúdez V, Serrano J.R., Piqueras P, Sanchis E.J. On the Impact of Particulate Matter Distribution on Pressure Drop of Wall-Flow Particulate Filters. Appl. Sci. 2017, 7, 234.
[69] M. Rößler, A. Velji, C. Janzer, T. Koch, M. Olzmann, Formation of Engine Internal NO 2 : Measures to Control the NO 2 /NO X Ratio for Enhanced Exhaust After Treatment, SAE Int. J. Engines. 10 (2017) 2017-01–1017. doi:10.4271/2017-01-1017.
[70] N. Singh, C.J. Rutland, D.E. Foster, K. Narayanaswamy, Y. He, Investigation into different DPF regeneration strategies based on fuel economy using integrated system simulation, SAE Tech. Pap. (2009). doi:10.4271/2009-01-1275.

Abbreviations

ATDC: After Top Dead Center

ATS: Aftertreatment System

CAD: Crank Angle Degree

CO: Carbon Monoxide

DI: Direct Injection

DOC: Diesel Oxidation Catalyst

DPF: Diesel Particulate Filter

DMDF: Dual Mode Dual Fuel

EGR: Exhaust Gas Recirculation

FSN: Filter Smoke Number

GCI: Gasoline Compression Ignition

GF: Gasoline Fraction

HC: Hydro Carbons

HCCI: Homogeneous Charge Compression Ignition

HR: Heat Release

HRF: High Reactivity Fuel

ICE: Internal Combustion Engine

IMEP: Indicated Mean Effective Pressure

LRF: Low Reactivity Fuel

LTC: Low Temperature Combustion

MCE: Multi Cylinder Engine

NOx: Nitrogen Oxides

OEM: Original Equipment Manufacturer

PFI: Port Fuel Injection

PPCI: Partially Premixed Compression Ignition

PRR: Pressure Rise Rate

RCCI: Reactivity Controlled Compression Ignition

RON: Research Octane Number

MON: Motor Octane Number

SCR: Selective Catalytic Reduction

S: Sensitivity